CemR atypical response regulator impacts energy conversion in *Campylobacteria*

Mateusz Noszka[1], Agnieszka Strzałka[2], Jakub Muraszko[1], Dirk Hofreuter[3], Miriam Abele[4], Christina Ludwig[4], Kerstin Stingl[5], Anna Zawilak-Pawlik[1*]

1 Department of Microbiology, Hirszfeld Institute of Immunology and Experimental Therapy, Polish Academy of Sciences, 53-114 Wrocław, Poland

2 Department of Molecular Microbiology, Faculty of Biotechnology, University of Wrocław, 50-383 Wrocław, Poland

3 Department of Biological Safety, Unit of Product Hygiene and Disinfection Strategies, German Federal Institute for Risk Assessment, 12277 Berlin, Germany

4 Bavarian Center for Biomolecular Mass Spectrometry (BayBioMS), Technical University of Munich (TUM), 85354 Freising, Germany

5 Department of Biological Safety, National Reference Laboratory for Campylobacter, German Federal Institute for Risk Assessment, 12277 Berlin, Germany

[*] Corresponding author

Email: anna.pawlik@hirszfeld.pl

Abstract

Campylobacter jejuni and *Arcobacter butzleri* are microaerobic food-borne human gastrointestinal pathogens that mainly cause diarrheal disease. These related species of the *Campylobacteria* class face variable atmospheric environments during infection and transmission, ranging from nearly anaerobic to aerobic conditions. Consequently, their lifestyles require that both pathogens need to adjust their metabolism and respiration to the changing oxygen concentrations of the colonization sites. Our studies revealed that *C. jejuni* and *A. butzleri* lacking a *Campylobacteria*-specific regulatory protein, *C. jejuni* Cj1608 or a homologue *A. butzleri* Abu0127, are unable to reprogram tricarboxylic acid cycle or respiration pathways, respectively, to produce ATP efficiently and, in consequence, adjust growth to changing oxygen supply. We propose that these *Campylobacterial* energy and metabolism regulators (CemR) are long-sought transcription factors controlling the metabolic shift related to oxygen availability, essential for these bacteria's survival and adaptation to the niches they inhabit.

Introduction

Campylobacter jejuni and *Arcobacter butzleri* are gram-negative, microaerobic bacteria that belong to the *Campylobacteria* class [1]. *C. jejuni* is a commensal bacterium of the gastrointestinal tracts of wildlife and domestic animals. However, in humans, *C. jejuni* is the leading cause of food-borne bacterial diarrheal disease [2]. Also, it causes autoimmune neurological diseases such as Guillian Barré and Miller–Fisher syndromes [3]. *A. butzleri* is found in many ecological niches, such as environmental water and animals. Still, in humans, *A. butzleri* causes diarrhea, enteritis, and bacteremia [2]. Due to the wide distribution of the two species and relatively high resistance to environmental conditions [4] and antibiotics [5,6], both species pose a severe threat to human health.

To adapt to different ecological niches and decide whether conditions are optimal for reproduction and transmission, *C jejuni* and *A. butzleri* encode numerous regulatory proteins. According to the MiST database [7], *C. jejuni* NCTC 11168 (1.64 Mbp; 1643 coding sequences [8]) and *A. butzleri* RM4018 (2.34 Mbp, 2259 coding sequences [9]) encode 56 and 218 signal transduction proteins, respectively. While *A. butzleri* regulatory systems have been hardly studied [10], the *C. jejuni* signal transduction systems have been partially deciphered [11–15]. Particular interest was directed to studying processes related to the *C. jejuni* colonization and focused on factors controlling the expression of genes involved in such processes as host adaptation and niche detection (BumSR, DccSR), oxidative stress (e.g., CosR, PerR), metabolism, and respiration (e.g., BumSR, RacSR, CosR, CsrA, LysR (Cj1000), CprSR) [11,13–15]. Notably, aerobic or microaerophilic respiration, in which oxygen is used as a terminal electron acceptor, is far more efficient in supplying energy than anaerobic respiration or fermentation [16]. On the other hand, oxygen-dependent respiration is a source of reactive oxygen species (ROS) [17]. *C. jejuni* requires oxygen for growth but, unlike facultative aerobic *A. butzleri*, is sensitive to aerobic conditions faced during transmission. In addition, *C. jejuni* and *A. butzleri* may encounter conditions deficient in oxygen in the intestine or during intracellular persistence [18]. Thus, *C. jejuni and A. butzleri* must adjust their metabolism and respiration as oxygen concentrations change at colonization sites to get sufficient energy while maintaining redox homeostasis. However, no orthologs of energy or redox metabolism regulators such as gammaproteobacterial ArcA, FNR or NarP are found in *C. jejuni* [14,19–21].

The roles of many *C. jejuni* and most *A. butzleri* regulators have still not been explored. One such regulator is the *C. jejuni* NCTC 11168 Cj1608 orphan response regulator, which is homologous to uncharacterized

A. butzleri RM4018 Abu0127. These regulators are homologous to *Helicobacter pylori* 26695 HP1021 and are conserved across most *Campylobacteria* class species, constituting most of the *Campylobacterota* phylum.

The *H. pylori* HP1021 response regulator is one of 28 signal transduction proteins encoded by *H. pylori* 26695 [7,22]. HP1021 interacts with the origin of chromosome replication region (*oriC*) *in vitro*, probably participating in the control of the initiation of *H. pylori* chromosome replication [23]. HP1021 acts as a redox switch protein, i.e. senses redox imbalance, transmits the signal and triggers the cells' response [24]. The HP1021 regulon, initially determined in *H. pylori* 26695 by microarray analyses [25], has been updated in *H. pylori* N6 using a multi-omics approach [26]. HP1021 influences the transcription of almost 30% of all *H. pylori* N6 genes of different cellular categories; the transcription of most of these genes is related to response to oxidative stress. HP1021 directly controls typical reactive oxygen species (ROS) response pathways and less canonical ones, such as central carbohydrate metabolism. The level of ATP and the growth rate of the knock-out *H. pylori* ΔHP1021 are lower than in the wild-type strain, which is possibly due to reduced transcription of many tricarboxylic acid cycle (TCA) genes and/or increased ATP consumption in catabolic processes in ΔHP1021 compared to the wild-type strain. Thus, HP1021, amongst many cellular processes, probably controls *H. pylori* metabolic fluxes to maintain the balance between anabolic and catabolic reactions, possibly for efficient oxidative stress response [26].

In this work, we focused on the two hardly characterized regulatory proteins of the microaerobic *C. jejuni* NCTC 11168 and the facultatively aerobic *A. butzleri* RM4018, Cj1608 and Abu0127, respectively. To get insight into the function of these proteins, we constructed mutants lacking these regulators and looked at transcriptomic and proteomic changes under optimal growth and oxidative stress conditions. Our results indicate that Cj1608 and Abu0127, which we named *Campylobacteria* energy and metabolism regulators (CemR), support energy conservation in bacterial cells by controlling metabolic and respiration pathways in response to oxygen availability.

Results

Influence of the Cj1608 regulator on *C. jejuni* gene and protein expression

Cj1608 have been hardly characterized thus far. It is only known that it interacts *in vitro* with the *C. jejuni oriC* region and the promoter of the *lctP* lactate transporter, probably participating in the control of the initiation of the *C. jejuni* chromosome replication and lactate metabolism [22,23]. Therefore, to elucidate the role of the Cj1608 regulator in controlling *C. jejuni* gene expression and oxidative stress response, we performed transcriptome analysis (RNA-seq) of the *C. jejuni* NCTC 11168 wild-type (CJ) and deletion mutant (ΔCj1608) strains under microaerobic growth (CJ, ΔCj1608) and during paraquat-induced oxidative stress (CJ_S, $\Delta Cj1608_S$) (S1A Fig).

A comparison of *C. jejuni* ΔCj1608 and CJ transcriptomes revealed 380 differentially transcribed genes (Figs 1A, 1B and S2A, S1 Data). The paraquat stress affected the transcription of genes in wild-type and ΔCj1608 strains (232 and 123 genes, respectively) (Figs 1B, S2B and S2C). The transcription of 44 genes was similarly induced or repressed in CJ_S and $\Delta Cj1608_S$ cells (S2D Fig, red dots). Thus, these genes responded to oxidative stress, but other or additional factors than Cj1608 controlled them. Using ClusterProfiler [27], we performed a KEGG enrichment analysis to identify processes affected most by the lack of Cj1608 or under stress. In the ΔCj1608 strain, three KEGG groups were activated (nitrogen metabolism, ribosomes, and aminoacyl-tRNA-biosynthesis). One KEGG group was suppressed, namely the tricarboxylic acid (TCA) cycle (Fig 1C). In the CJ strain under stress conditions, six KEGG groups were suppressed (e.g., oxidative phosphorylation), while four KEGG groups were activated (e.g., carbon metabolism).

Since post-transcriptional regulation is common in bacteria, including species closely related to *C. jejuni* [28,29], a proteomics approach (LC-MS/MS) was applied to detect proteins whose levels changed between analyzed strains or conditions. A total of 1170 proteins were detected (S1 Data); however, 173 proteins encoded by genes whose transcription changed in ΔCj1608 were not detected by MS (S1 Data). The comparison between proteomes of ΔCj1608 and CJ strains under microaerobic conditions revealed different levels of 156 proteins (S4A Fig, red, yellow, and green dots). The transcriptomic and proteomic data correlated strongly (Figs S5A and 1D, red dots). However, the differences between transcription and translation patterns were observed for many genes, suggesting a post-transcriptional regulation of *C. jejuni* gene expression (Fig 1D, blue, yellow, and green dots). Under oxidative stress, the expression of only four genes changed, namely, the

expression of ferrochelatase HemH (Cj0503c) was downregulated in the CJ_S cells; at the same time, the levels of three proteins were up-regulated (the catalase KatA (Cj1385), the atypical hemin-binding protein Cj1386, mediating the heme trafficking to KatA [30], and the periplasmic protein Cj0200c) (Figs S4B and S4C). The small number of proteins whose expression was altered under oxidative stress confirmed the known phenomenon of ceasing protein synthesis by bacteria under oxidative stress [26,31]. The ClusterProfiler KEGG enrichment analysis revealed that genes of two KEGG groups, nitrogen metabolism and ribosome, were activated in the ΔCj1608 strain in comparison to CJ, while the genes of three KEGG groups were suppressed (TCA cycle, ABC transporters and carbon metabolism) (Fig 1E). It should be noted that the nitrogen metabolism group includes proteins such as GlnA and GltBD, which are involved in glutamate metabolism and TCA cycle [32], whose levels increased more than 10-fold, and Nap and Nrf complexes, constituting an electron transport chain (ETC) system (see below).

To conclude, the transcriptomic and proteomic data revealed that Cj1608 impacts the transcription of 585 genes and the expression of 156 proteins in *C. jejuni* NCTC 11168, with the TCA and nitrogen metabolism KEGG groups most affected.

Influence of Abu0127 on *A. butzleri* gene and protein expression

To elucidate the role of the Abu0127 regulator in controlling gene expression and oxidative stress response of *A. butzleri,* we performed RNA-seq and LC-MS/MS analyses similar to those for *C. jejuni*. We analyzed gene expression in *A. butzleri* RM4018 wild-type (AB) and deletion mutant (ΔAbu0127) strains; paraquat was used to induce oxidative stress (AB_S, $\Delta Abu0127_S$) (S1B Fig [33]).

Comparison of *A. butzleri* ΔAbu127 and AB transcriptomes revealed 779 differentially transcribed genes (Figs 2A, 2B and S3A, S2 Data). The paraquat stress affected the transcription of genes in the wild-type and, to a much lesser extent, in the ΔCj1608 strain (290 and 14 genes, respectively) (Figs 2B, S3B and S3C). 12 of these 14 differently transcribed genes in ΔCj1608 strain were also induced in AB_S cells (S3D Fig, red dots). Thus, these genes responded to oxidative stress but were controlled by factors other than or additional to Abu0127. KEGG enrichment analysis revealed that in the ΔAbu0127 strain, two KEGG groups were activated, ABC transporters and sulfur metabolism, while 13 groups were suppressed (e.g., oxidative phosphorylation and TCA cycle) (Fig 2C). In the AB strain under stress conditions, seven KEGG groups were suppressed (e.g., oxidative phosphorylation and citrate cycle), while six groups were activated (e.g., sulfur metabolism).

As in our *C. jejuni* study, a proteomic approach was used to detect proteins whose levels changed between the strains and conditions analyzed. 1586 *A butzleri* proteins were detected (S2 Data). However, proteomics did not detect 224 proteins encoded by genes whose transcription changed in ΔAbu0127 (S2 Data). The comparison between proteomes of ΔAbu0127 and AB strains under microaerobic conditions revealed 124 differentially expressed proteins (Figs 2D and S4D, red, yellow, and green dots). As in *C. jejuni* studies, the transcriptomics and proteomics data correlated (Figs S5B and 2D, red dots); however, in cases of many genes post-transcriptional modifications probably affected the final protein levels in the *A. butzleri* cell (Fig 2D, blue, yellow, and green dots). Under paraquat stress, the level of only one protein changed. Namely, Abu0530, of unknown function, was produced at a higher level in AB_S cells compared to AB cells (Figs S4E and S4F). Thus, *A. butzleri,* like *C. jejuni* ceased protein translation upon oxidative stress, which is also typical for other bacterial species [34]. The transcriptomics and proteomics data correlated strongly (Fig S5B). The ClusterProfiler KEGG enrichment analysis revealed that genes of one KEGG group, sulfur metabolism, were activated in the ΔAbu0127 strain compared to AB. In contrast, the genes of three KEGG groups were suppressed (oxidative phosphorylation, taurine and hypotaurine metabolism, ribosome) (Fig 2E).

To conclude, the results of transcriptomic and proteomic analyses indicated that Abu0127 affects the transcription of 904 genes and the expression of 124 proteins in *A. butzleri* RM4018, with the oxidative phosphorylation KEGG group most affected.

Cj1608 and Abu0127 are involved in the regulation of energy production and conversion

The transcriptome and proteome analyses of both species revealed that the energy production and conversion processes, such as the TCA cycle and oxidative phosphorylation, are putatively controlled in *C. jejuni* by Cj1608 and in *A. butlzeri* by Abu0127 (S1 Data, S2 Data and S3 Data). In *C. jejuni* ΔCj1608, the protein levels of all but two TCA enzymes, fumarate reductase FrdABC and fumarate hydratase FumC, decreased, with the citrate synthase GltA protein level reduced by as much as 70-fold (Figs 3A and S6; the level of oxoglutarate-acceptor oxidoreductase Oor was reduced by 1.7-2-fold). Many genes encoding nutrient importers and downstream processing enzymes were down-regulated in *C. jejuni* ΔCj1608 (e.g., amino acid ABC transporter permease Peb, fumarate importer DcuAB, L-lactate permease LctP and lactate utilization proteins Lut). However, DctA succinate/aspartate importer and the enzymes glutamine synthetase GlnA and glutamate synthase small subunit GltB involved in glutamine and glutamate synthesis were up-regulated (Fig

169 3A). The levels of many proteins forming ETC complexes were also down-regulated, including subunits of
170 NADH-quinone oxidoreductase Nuo and cytochromes (Fig 3B). In *A. butzleri* ΔAbu0127, the levels of GltA
171 and isocitrate dehydrogenase Icd proteins were reduced (Figs 3C and S7C). As in *C. jejuni*, the levels of many
172 proteins forming ETC complexes decreased, with Nuo complex subunits being the most highly downregulated
173 (Figs 3D, S7A and S7B).

174 Moreover, a functional analysis annotation with eggNOG-mapper, indicated the Clusters of Orthologous
175 Groups (COG) of differentially expressed genes and proteins. In both species, the most variable groups
176 belonged to two categories, namely energy production and conservation (C) and translation, ribosomal
177 structure, and biogenesis (J) (Fig 4, the category of unknown genes was excluded from the graph, S1 Data and
178 S2 Data). Many genes and proteins suppressed in both species belong to the energy production and conversion
179 group.

180 These comprehensive data suggest that mutants of both species produce less energy due to the inhibition of
181 the TCA cycle and oxidative phosphorylation. Therefore, we decided to investigate these processes in more
182 detail and analyze how the lack of Cj1608 and Abu0127 proteins influences energy production and conversion
183 in *C. jejuni* and *A. butzleri*, respectively.

184

185 **Cj1608 controls *gltA* expression, ATP level and growth in response to O_2 supply**

186 To analyze the influence of Cj1608 on *C. jejuni* growth, we compared the growth of wild-type CJ, knock-
187 out ΔCj1608 and complementation (C_{Cj1608}) strains (Fig 5A). It should be noted that unless an accessory ETC
188 electron donor and proton motive force generator H_2 was supplied in the microaerobic gas mixture (4 % H_2,
189 Materials and Methods) (see also [35]), we could not obtain the ΔCj1608 mutant strain of *C. jejuni* NCTC
190 11168. When *C. jejuni* was cultured microaerobically in the presence of H_2, the growth of *C. jejuni* ΔCj1608
191 was slower (i.e., the generation time (G) was higher) than the CJ and C_{Cj1608} strains (Fig 5A). The ΔCj1608
192 culture entered the stationary phase at optical density (OD) like that of CJ and C_{Cj1608}strains (Fig 5A). Under
193 microaerobic conditions without H_2, the CJ and C_{Cj1608}strains grew similarly to conditions with H_2, albeit
194 reaching lower OD_{600} at the stationary phase than with H_2 (Fig 5A). In contrast, the ΔCj1608 strain almost did
195 not grow without H_2, confirming that its growth strictly depended on hydrogen. The ATP analysis indicated
196 that the relative energy levels corresponded to the bacterial growth rates. The ATP level of the CJ strain under
197 microaerobic growth without H_2 was assumed to be 100% (Fig 5B). The ATP level in CJ and C_{Cj1608}strains was

constant regardless of the presence or absence of H_2 (85% - 100%). Without H_2, the ATP level in the ΔCj1608 strain dropped to 25 ± 4% of the ATP level in the CJ strain. In the presence of H_2, the level of ATP in ΔCj1608 cells increased to 53 ± 8 % compared to that of the CJ strain. These results indicated that the availability of additional electrons and proton motive force (PMF) derived from hydrogen [35], an alternative to those produced by the TCA cycle and used in oxidative phosphorylation, enabled ΔCj1608 cells to produce more energy and multiply more efficiently.

Next, we analyzed whether Cj1608 directly affects the TCA cycle efficiency, as suggested by hydrogen boost analysis. We studied the expression of *gltA* since the expression of this gene was severely downregulated in the ΔCj1608 strain (Figs S8A and S8B, S3 Data). GltA is the first enzyme in the TCA cycle whose activity impacts the flow of substrates through the TCA cycle and energy production via NADH/FADH/menaquinone cofactors (Fig 3A). It was previously shown that *gltA* transcription depends on the O_2 concentration, being lower at 1.88% O_2 and higher at 7.5% O_2, which helps *C. jejuni* optimize energy production and expense during different oxygen availability as the electron acceptor [36]. Here, we confirmed the specific interaction of the Cj1608 protein with the *gltA* promoter region *in vivo* by chromatin immunoprecipitation (ChIP) and *in vitro* by electrophoretic mobility shift assay (EMSA) (Figs 5C and 5D); Cj1608 did not interact with a control *C. jejuni recA* region. Next, we used RT-qPCR to analyse *gltA* transcription under oxidative stress triggered by paraquat or under diverse O_2 availability: reduced 1% O_2, optimal microaerobic 5% O_2 and increased 10% O_2 (Materials and Methods). Transcription of *gltA* was lower in ΔCj1608 than in CJ and C_{Cj1608}strains under optimal conditions (FC of 0.14 ± 0.14) and unaffected by paraquat stress, confirming the transcriptomic results (S8C Fig). Moreover, transcription of *gltA* was upregulated in the CJ and C_{Cj1608}strains at 5% O_2 compared to 1% O_2 (Fig 5E). However, in CJ and C_{Cj1608} strains, the *gltA* transcription was down-regulated at 10% O_2 compared to 5% O_2 (Fig 5E), suggesting that the prolonged bacterial growth for 5 hours at increased O_2 concentration possibly caused adaptation to higher oxygen level conditions or stress by reducing TCA cycle activity and possible ROS production during increased aerobiosis. However, *gltA* transcription was constant in ΔCj1608 at all O_2 concentrations, indicating that cells could not adjust *gltA* transcription to changing O_2 conditions. Next, we analyzed *C. jejuni* growth and ATP production under various O_2 supplies. Under 1% O_2, the ΔCj1608 strain grew faster than WT and C_{Cj1608} strains, suggesting that the metabolic state of the ΔCj1608 mutant strain was optimized for reduced O_2 concentration (Fig 5G). Under optimal O_2 level, CJ and C_{Cj1608} strains grew faster than under 1% O_2 and faster than the ΔCj1608 strain under 5% O_2, indicating that metabolic

pathways of CJ and C_{Cj1608} strains were adjusted to increased O_2 availability, while the metabolism of ΔCj1608 was not. Under increased O_2 concentration, all three strains grew slower than under optimal conditions, with the ΔCj1608 strain growing slower than the CJ and C_{Cj1608} strains. The ATP analyses indicated that the relative ATP levels corresponded to the bacterial growth rates. The ATP level of the CJ strain under optimal microaerobic growth was assumed to be 100%. Compared to that, the level of ATP in the CJ strain under reduced O_2 concentration dropped to 38 ± 4%; at increased O_2 concentration, the level of ATP also decreased to 51 ± 7% (Fig 5F, see Discussion). Under optimal conditions in the ΔCj1608 mutant strain, the ATP level reached approximately 70 ± 8% of that in the CJ strain and was constant regardless of increased or decreased O_2 supply. The ATP levels in the C_{Cj1608}strain analyzed at different O_2 levels resembled that of the CJ strain. Thus, the results indicated that the ΔCj1608 mutant strain could not adjust pathways responsible for energy conservation to changing O_2 levels.

To summarize *C. jejuni*'s results, Cj1608 helps *C. jejuni* control pathways that are important for energy conservation and are dependent on oxygen availability. As we have shown using the *gltA* gene as an example, Cj1608 directly controls gene expression in response to changing O_2 concentrations and oxidative stress.

Abu0127 controls *nuo* expression, ATP level and growth in response to O_2 supply.

Next, we examined the impact of Abu0127 on *A. butzleri's* growth. As for *C. jejuni*, the presence or absence of H_2 did not significantly affect the growth of the wild-type AB strain nor ATP level in AB cells under microaerobic conditions (Fig 6A). In the presence of H_2, the ΔAbu0127 strain grew slower than the AB strain (Fig 6A), and the ATP level of ΔAbu0127 cells reached 77± 3% of that in the WT cells (Fig 6B). However, the ΔAbu0127 culture entered the stationary phase at OD_{600} comparable to that of the AB strain. Under microaerobic conditions without H_2, the growth and ATP level of ΔAbu0127 was further lowered; ΔAbu0127 ATP level reached 57 ± 3% of the AB cells and cells entered stationary phase at lower OD_{600} than the wild-type AB strain (Figs 6A and 6B). Despite many attempts, we could not construct an Abu0127 complementation mutant, possibly due to the imperfect molecular biology tools dedicated to *A. butzleri* [10]. Nonetheless, the results indicated that the ΔAbu0127 strain produced less energy than AB cells, and using H_2, the ΔAbu0127 cells could produce more energy and multiply more efficiently [35]. This suggests a similar pattern of bypass of TCA-dependent energy production via oxygen-dependent oxidative phosphorylation to that observed in *C. jejuni*.

Next, we analyzed whether Abu0127 directly affects the Nuo complex activity. We studied the expression of *nuoB* since it is the second gene of the *nuoA-N* operon, whose expression was severely downregulated in the ΔAbu0127 strain at the transcription and translation level (Figs S9A and S9B, S3 Data). We confirmed the interaction of the Abu0127 protein with the *nuoA-N* promoter region *in vivo* by ChIP-qPCR and *in vitro* by EMSA (Figs 6C and 6D), and we figured that it was specific because Abu0127 did not interact with control *A. butzleri gyrA* and *recJ* regions. Next, we used RT-qPCR to analyse *nuoB* transcription under paraquat-induced oxidative stress and different O_2 supply, as previously in *C. jejuni*. It should be noted that *A. butzleri* can grow under aerobic conditions [37]; thus, aerobic O_2 concentration is less harmful to *A. butzleri* than to *C. jejuni*. The transcription of *nuoB* changed across different O_2 concentrations, being the lowest at 1% O_2 (FC of 0.61 ± 0.06 compared to AB under 5% O_2) and highest at 10%O_2 (FC of 1.7 ± 0.27 compared to AB under 5% O_2) (Fig 6E). Under optimal O_2 conditions, *nuoB* transcription was lower in the ΔAbu0127 strain than in the AB strain (FC of 0.3 ± 0.05 compared to AB under 5% O_2), and it was invariant across different O_2 concentrations (Fig 6H). Paraquat-induced oxidative stress affected *nuoB* transcription neither in the wild-type AB nor ΔAbu0127 strain, confirming the transcriptomic results (Figs S9C, S3 Data). Next, we analyzed *A. butzleri* growth and ATP production under various O_2 supplies. Under 1% O_2, the AB and ΔAbu0127 strains grew similarly. However, ΔAbu0127 reached a lower OD_{600} at the stationary growth phase than the AB strain (Fig 6F). Under optimal and increased O_2 concentrations, the AB strain grew similarly at both concentrations, faster than under 1% O_2, but reached a similar OD_{600} upon entry to a stationary growth phase as under 1% O_2. The ΔAbu0127 strain grew similarly under 5% and 10% O_2 but faster than under 1% O_2. Nonetheless, ΔAbu0127 grew slower than AB under the same conditions, and the culture finally reached a lower OD_{600} than AB (Fig 6F). The relative ATP energy levels corresponded to the bacterial growth rates. The ATP level of the AB strain under microaerobic growth was assumed to be 100%. Compared to that, under 1% O_2, the level of ATP in the AB strain dropped to 44 ± 4%, while the level of ATP did not change in the culture grown at 10% O_2 (Fig 6G). Under reduced O_2 concentration, the level of ATP in ΔAbu0127 was similar to that of the AB strain under the same conditions (35 ± 4% compared to AB under microaerobic growth). However, under 5% O_2, the ATP level of the ΔAbu0127 mutant strain reached 76 ± 3% of that in the AB strain and did not increase under 10% O_2. Thus, the results indicated that the ΔAbu0127 mutant strain could not efficiently adjust pathways responsible for energy conservation to changing O_2 levels, in which it resembled *C. jejuni* ΔCj1608.

To summarize *A. butzleri*'s results, Abu0127 helps *A. butzleri* control pathways important for energy conservation dependent on oxygen availability. As we have shown using the *nuoB* gene as an example, Abu0127 directly controls gene expression in response to changing O_2 concentrations.

Discussion

One of the challenges for a bacterial cell is to gain energy to grow and reproduce under different environmental conditions. Available energy sources and electron acceptors used for energy conversion are the two major factors defining the activity of metabolic pathways. The regulatory proteins redirect metabolism and ETC pathways, prioritizing electron donor or acceptor usage to maximize the energy gain (e.g., aerobic/microaerophilic over anaerobic respiration and fermentation or nitrate respiration over fumarate respiration). The fine-tuning of metabolism and respiration to particular conditions is usually hierarchical and orchestrated by multiple factors [38,39], which often control the same genes. For example, in the model, facultative anaerobe *E. coli*, but also other species of *Gammaproteobacteria*, three global transcriptional regulators, FNR, ArcA and NarL/NarP, mainly control energy conservation processes dependent on electron acceptors availability[21,40]. In the energy reprogramming network, under low oxygen availability, FNR provides the first level of regulation, switching metabolism from aerobic to anaerobic and controlling the expression of other transcriptional factors [41]. ArcA, a response regulator of the ArcAB two-component system [42], possibly controls the switch between anaerobic respiration and fermentation as well as the expression of a set of secondary regulators [43]. NarL/NarP switches on nitrate and nitrite respiration when these electron acceptors are available while repressing genes for less effective anaerobic respiration [44]. Studies have shown that the intensive cross-talk between regulatory proteins, often controlling the same genes hierarchically and controlling genes beyond energy conservation pathways, is essential for efficient bacterial responses or adaptation to diverse conditions [21,45–47].

Until recently, no regulators redirecting energy conversion pathways in response to oxygen as an electron acceptor have been found in *Campylobacterota* [14,48]. It was experimentally shown that *C. jejuni* reprograms its metabolism upon changes to oxygen availability; nonetheless, the regulator remained unknown [36,49]. It was surprising given that microaerobic species of this phylum must respond to changing oxygen levels, including harmful oxygen deficiency and excess.

In this and previous works [24,26], we revealed that under microaerobic conditions, three homologous atypical response regulators, HP1021, Cj1608 and Abu0127, which we name *Campylobacteria* energy and metabolism regulators (CemR), control the expression of many genes involved in energy conversion, including TCA and ETC pathways (Figs 3, 4 and S10, Supplementary Data 3 in [26]). Indeed, when *cemR* genes were

deleted, the most remarkable gene and protein expression changes occurred in energy production and conversion COG, reaching between 20 to 40% of all the down-regulated genes or proteins (Figs 4 and S10, the category of unknown proteins was excluded from the study). Moreover, we showed that in strains lacking CemR, the transcriptional control was lost over the genes whose transcription was dependent on the oxygen level, e.g., *C. jejuni* TCA *gltA*, *A. butzleri* ETC *nuoA-N* operon complex, *H. pylori,* TCA pyruvate:ferredoxin oxidoreductase *PFOR* and ETC cytochrome c oxidase *ccoN-Q* (Figs 5E, 6E and [26]). Consequently, under microaerobic conditions in CemR deletion mutants of all three species, the ATP level and the growth rates were lower than in wild-type strains (Figs 5F, 5G, 6F 6G and Fig 3E in [26]). The presence of CemR allowed *C. jejuni* and *A. butlzeri* to optimize energy conservation under microaerobic compared to reduced oxygen concentration, increasing the ATP level and bacterial growth rate (Figs 5F, 5G, 6F and 6G). The lack of CemR specifically impaired pathways connected with oxygen utilisation as an electron acceptor because in the presence of hydrogen as an alternative electron donor and proton motive force generator, *C. jejuni* and *A. butzleri* gained additional energy, allowing for faster growth (Figs 5A, 5B, 6A and 6B). All these data indicate that CemR responds to oxygen levels and redirects metabolism towards optimal energy conservation. It is important to point out that data obtained from each single species would not have allowed us to conclude on the general role of CemR as an energy conservation regulator because, in each species, slightly different pathways were primarily controlled (e.g., TCA in *C. jejuni*, Nuo ETC in *A. butzleri* and glucose uptake and pentose phosphate pathway in *H. pylori*). Nonetheless, the role of CemR in controlling other pathways or processes, often in a species-specific manner, still awaits detailed characterization.

An interesting question arises: how many energy conservation regulators are encoded in addition to CemR in each *Campylobacteria* species, and how do they all integrate into the regulatory circuits of a given species? *H. pylori*, *C. jejuni* and *A. butzleri* differ in lifestyles, which shape the complexity of regulatory circuits, as recently illustrated using *Campylobacterota* as a representative phylum [50]. *H. pylori* can be classified as a specialist bacterium [51] - strictly human-associated, using a limited repertoire of electron donors (hydrogen, pyruvate, 2-oxo-glutarate, malate, and succinate) and only oxygen or fumarate as electron acceptors during respiration [20]. Oxygen, being a primary electron acceptor in *H. pylori*, is also toxic for *H. pylori* at higher than microaerobic concentrations [52]. As a consequence of speciation and host adaptation, *H. pylori* lost many regulatory proteins. Nonetheless, the studies on regulatory circuits in *H. pylori* indicated that HP1043 [53,54], controlled by unknown stimuli, acid-responsive ArsRS [55], and metal-dependent regulators NikR and Fur

[20,56], affect *H. pylori* energy conversion to various extents in response to different stimuli. *C. jejuni* is a host-associated organism that infects various animals and humans and can survive long periods under aerobic conditions [57]. In contrast to *H. pylori*, *C. jejuni* has a branched electron transport chain with multiple enzymes that utilize more molecules as electron donors and acceptors than *H. pylori* [20]. *C. jejuni* genome size is similar to *H. pylori*; however, the number of *C. jejuni* genes encoding regulatory proteins is higher and reflects the broader spectrum of ecological niches inhabited by this bacterium. Consequently, the number of regulatory proteins controlling energy conversion is higher than in *H. pylori,* with RacRS, LysR (Cj1000), CsrA and CprRS playing the most significant roles (for details, see reviews [11,13–15]). Depending on growth conditions, particularly the availability of electron donors and acceptors, LysR, RacRS, and CprRS regulate the expression of fumarate respiration genes, which is an excellent example of a cross-talk between regulators controlling the same pathways via transcriptional control over the same genes (e.g., *aspA, dcuA, mfr* or *frd*) [48,58,59]. RNA-binding CsrA, a homologue of *E. coli* carbon starvation regulator, is an example of post-transcriptional energy conservation regulation in *C. jejuni,* including control of expression of TCA and ETC genes [60]. *A. butzleri* can lead anaerobic, microaerophilic, and aerobic lifestyles as an environmental or animal- and human-associated bacterium. As a generalist, it utilizes many electron donors and acceptors using an electron transport chain similar to those used by the free-living marine *Campylobacterota* [20]. *A. butzleri*'s genome encodes many signal transduction proteins (see Introduction), including extracytoplasmic sigma factors (ECFσ) to adapt to different conditions. However, hardly anything is known about the regulation of *A. butzleri* energy conversion except that a few species of ECFσ impact electron and carbon metabolism by affecting the transcription of genes from carbon metabolism pathways and electron acceptor complexes [10]. However, one can expect the highest complexity and speciation of *A. butzleri*'s regulatory circuits, including energy conservation, of all three species.

CemR regulators are highly conserved *Campylobacteria* regulators. However, the molecular mechanism of signal perception by CemR is still enigmatic and cannot be predicted by analogy. Transcriptional regulatory proteins may sense respiration status, the concentrations of electron donors or acceptors, or respiration byproducts [61]. We have shown that cysteine residues of HpCemR become oxidized under O_2-triggered oxidative stress *in vivo* and *in vitro*, which changes the protein's DNA-binding activity possibly by structural changes of DNA-protein complex rather than on-off mechanism [24,26]. Recent studies on CjCemR interactions with the promoter region of *lctP* suggested a similar mechanism of CjCemR activity control and

lctP transcription regulation [62]. AbCemR protein also contains cysteine residues, one of which is conserved in all three species (C27 in HpCemR and CjCemR, C31 in AbCemR). The mechanism of activity regulation by the redox state of the cysteine residues resembles that of ArcA-ArcB two-component system regulation. However, in that TCS, the cysteine residues of ArcB sensor kinase are oxidated, triggering autophosphorylation of ArcB, while ArcA response regulator is activated by phosphorylation. CemR proteins are orphan atypical response regulators in which the same molecule receives and executes the signal. Thus, despite some biochemical similarity to ArcAB system activation, the exact molecular mechanism of CemR activity control has not yet been discovered.

In summary, CemR, the global regulatory protein, is a part of the cell response to a metabolic redox imbalance, either caused by environmental conditions such as oxygen availability or ROS or triggered intracellularly due to metabolic changes and increased ROS production. However, the exact pathway of signal transduction by CemR and the levels or hierarchy of regulation are still unknown. Further comprehensive, multi-omic studies are needed to reveal the complex circuits of regulation involving CemR and other regulatory proteins in *Campylobacteria* energy conservation.

Materials and methods

Materials and culture conditions

The strains, plasmids and proteins used in this work are listed in the S1 Table. The primers used in this study are listed in the S2 Table. *C. jejuni* and *A. butzleri* plate cultures were grown on Columbia blood agar base medium supplemented with 5% defibrinated sheep blood (CBA-B). The liquid cultures were prepared in Brain Heart Infusion Broth (BHI) (Oxoid) and incubated with 140 rpm orbital shaking. All *C. jejuni* and *A. butzleri* cultures were supplemented with antibiotic mixes (*C. jejuni*: vancomycin (5 µg/ml), polymyxin B (2.5 U/ml), trimethoprim (5 µµg/ml) and amphotericin B (4 µg/ml) [63]; *A. butzleri*: cefoperazone (8 µg/ml), amphotericin (10 µg/ml), teicoplanin (4 µg/ml) [64]). If necessary for selecting mutants, appropriate antibiotics were used with final concentrations (i) kanamycin 20 µg/ml (*C. jejuni* and *A. butzleri*), (ii) chloramphenicol 8 µg/ml (*C. jejuni*). Routinely, *C. jejuni* and *A. butzleri* were cultivated at 42°C or 30°C, respectively under optimal microaerobic conditions (*C. jejuni*: 5% O_2, 8% CO_2, 4% H_2 and 83 % N_2; *A. butzleri*: 6% O_2, 9% CO_2, and 85% N_2) generated by the jar evacuation-replacement method using Anaerobic Gas System PetriSphere. The gas mixtures were modified by lowering or increasing O_2 and H_2 concentrations for ATP assays and growth curve analyses. Briefly, bacteria were cultured under microaerobic conditions optimal for each species to the late logarithmic growth phase (OD_{600} ~0.8), diluted to OD_{600} ~0.05 and incubated under the desired atmosphere as long as required, up to OD_{600} = 0.2-0.6 for ATP and RT-qPCR or until late stationary phase in growth analyses. The gas mixture with or without H_2 was composed of optimal gas mixtures for *C. jejuni* and *A. butzleri*, respectively. Low oxygen gas mixture was composed of 1% O_2, 10% CO_2, 5% H_2 and 84% N_2, while high oxygen gas mixture was composed of 10% O_2, 5% CO_2, 3% H_2 and 82% N_2. *Escherichia coli* DH5α and BL21 were used for cloning and recombinant protein synthesis. If necessary for selecting *E. coli,* appropriate antibiotics were used with final concentrations (i) kanamycin 50 µg/ml and (ii) ampicillin 100 µg/ml.

Construction of *C. jejuni* mutant strains

C. jejuni mutant strains were constructed using a homologous recombination and natural transformation approach [65]. *C. jejuni* NCTC 11168 was grown in 12 ml BHI to an OD_{600} = 0.2. Next, 150 µl of the culture was centrifuged and resuspended in fresh 150 µl of BHI. 150 ng (1 µg/ml) of EcoRI methylated plasmid was added to the culture and cultivated at 42 °C in microaerobic (3.75% H_2, 5.25% O_2, 7.5% CO_2) conditions with

shaking (140 rpm) for 4 h. Next, 100 µl was spread on CBA-B plates with an appropriate antibiotic and incubated for 3 days at 42 °C under microaerobic (3.75% H_2, 5,25% O_2, 7,5% CO_2) conditions.

C. jejuni NCTC 11168 ΔCj1608

The *C. jejuni Cj1608* deletion construct (pCR2.1/ΔCj1608) was prepared as follows (S11A Fig). The upstream and downstream regions of *Cj1608* were amplified by PCR using the P1-P2 and P5-P6 primer pairs, respectively and a *C. jejuni* NCTC 11168 genomic DNA as a template. The *aphA-3* cassette was amplified using the P3-P4 primer pair; pTZ57R/TΔHP1021 [23] was used as a template. The resulting fragments were purified on an agarose gel. Subsequently, the fragments were combined into one DNA amplicon with an overlap extension PCR reaction using the P1-P6 primers. The generated amplicon was purified on an agarose gel and cloned to the pCR2.1-TOPO® plasmid (Thermo Fisher Scientific) according to the manufacturer protocol. The DNA fragment cloned in pCR2.1-TOPO® was sequenced. Subsequently, *C. jejuni* NCTC 11168 was transformed with the pCR2.1/ΔCj1608 plasmid, and the transformants were selected by plating on CBA-B plates supplemented with kanamycin. The addition of hydrogen was necessary to obtain the kanamycin-resistant colonies. The allelic exchange was verified by PCR using the P7-P8 primer pair. The lack of *Cj1608 in C. jejuni* NCTC 11168 ΔCj1608 was confirmed by RNA-seq (S11B Fig), LC-MS/MS (S1 Data) and Western blot (Figs S11C and S11D).

C. jejuni NCTC 11168 C_{Cj1608}

The *C. jejuni Cj1608* complementation construct (pUC18/COMCj1608) was prepared as follows (S11A Fig). The regions upstream and downstream of the *Cj1608* gene were amplified by PCR using the P1-P6 primer pair and *C. jejuni* Cj1608 genomic DNA as a template. The resulting fragment was purified on an agarose gel. Subsequently, the generated amplicon and the SmaI digested vector pUC18 were ligated according to the method described by Gibson et al.[66] to give pUC18/COMCj1608. *E. coli* DH5α competent cells were transformed with the construct by heat shock. The insert cloned into pUC18 was sequenced. The pUC18/COMCj1608 was used to complement the lack of *Cj1608* in *C. jejuni* NCTC 11168 ΔCj1608 by an attempt similar to Multiplex Genome Editing by Natural Transformation (MuGENT) [67]. For the selection, a pSB3021 suicide plasmid was used. The plasmid harbors a *cat* cassette flanked by arms of homology, enabling *cat* cassette integration into the *hsdM* gene. Subsequently, the obtained pUC18/COMCj1608 (1 µg/ml) and

pSB3021 (0.25 µg/ml) plasmids were used in the natural transformation of *C. jejuni* NCTC 11168 ΔCj1608. The transformants were selected by plating on CBA-B plates supplemented with chloramphenicol. The bacteria were cultured without hydrogen to increase the selection process. The allelic exchange was verified by PCR using the P7-P9 primers. The presence of *Cj1608* in *C. jejuni* NCTC 11168 $C_{Cj1608}$was confirmed by RNA-seq (S11B Fig), LC-MS/MS (S1 Data) and Western blot (Figs S10C and S10D).

Construction of *A. butzleri* mutant strain

A. butzleri RM4018 mutant strain was constructed using a homologous recombination and electroporation approach. *A. butzleri* was grown in 25 ml BHI to an OD_{600} = 0.4. Next, the culture was transferred on ice and left for 10 min, then centrifuged (4,700 g, 10 min, 4 °C) and washed twice with 20 ml of ice-cold glycerine water (15% glycerol, 7% sucrose, filtrated). Finally, the culture was suspended in 250 µl of ice-cold glycerine water. For electroporation, 50 µl of electrocompetent cells were mixed with 5 µg of appropriate plasmid. Electroporation was performed in 0.1 cm electroporation cuvettes (The Cell Projects) using a Gene Pulser II Electroporator (Bio-Rad) using the following parameters – 12.5 kV/cm, 200 Ω, 25 µF. Cells were regenerated by adding 1 ml of BHI medium to the cuvette, then by transferring the cells to a flask with 2 ml BHI and cultivated with shaking (140 rpm) for 4 hours at 30 °C in microaerobic conditions. Next, the culture was centrifuged (4,700 g, 10 min, 22 °C), resuspended in 100 µl of BHI, spread on CBA-B plates with appropriate antibiotic and incubated for 5 days at 30 °C under microaerobic conditions.

A. butzleri RM4018 ΔAbu0127

The *A. butzleri Abu0127* deletion construct (pUC18/ΔAbu0127) was prepared as follows (S12A Fig) [68]. The upstream and downstream regions of *Abu0127* were amplified by PCR using the P10-P11 and P14-P15 primer pairs, respectively, and an *A. butzleri* RM4018 genomic DNA as a template. The *aphA-3* cassette was amplified using the P12-P13 primer pair; pTZ57R/TΔHP1021[23] was used as a template. The resulting fragments were purified on an agarose gel. Subsequently, the PCR-amplified fragments and the SmaI digested vector pUC18 were ligated according to the method of Gibson et al. [66]. Subsequently, *A. butzleri* RM4018 was transformed via electroporation with the pUC18/ΔAbu0127 plasmid, and the transformants were selected by plating on CBA-B plates supplemented with kanamycin. The allelic exchange was verified by PCR using the P16-P17

primer pair. The lack of *Abu0127* in *A. butzleri* RM4018 ΔAbu0127 was confirmed by RNA-seq (S12B Fig), LC-MS/MS (S2 Data) and Western blot (Figs S12C and S12D).

Disc diffusion assay

Bacteria were cultured in BHI to OD_{600} = ~0.5-0.7 and then diluted to OD_{600} = 0.1 in BHI. Each culture was spread by a cotton swab on CBA-B plates. Sterile, glass fibre 6-mm discs were placed on plates, and 5 µl of tested solutions were dropped on discs: 2% H_2O_2 (POCH, 885193111), 2% paraquat dichloride (Acros Organics, 227320010), 5% hydroxyurea (Merck, H8627-1G), 3% sodium nitroprusside (Merck, S0501), 2.5% menadion (Merck, A13593) and 15% sodium hypochlorite (Merck, 1056142500). Sodium hypochlorite solutions for assays were made fresh; the solutions' pH was adjusted by adding HCl to pH 7 and kept in PBS buffer prior to experiments [69]. Menadion solution was prepared in DMSO. The diameter of the inhibition zone around the discs was determined after 3 days of incubation under microaerobic conditions. The experiment was performed using three biological replicates.

RNA isolation

Bacterial cultures (12 ml BHI) of *C. jejuni* and *A. butzleri* strains were grown under microaerobic conditions to OD_{600} of 0.5-0.6. Immediately after opening the jar, 2 ml of the non-stressed culture was added to 2 ml of the RNAprotect Bacteria Reagent (Qiagen), vortexed and incubated for 5 min at room temperature. In parallel, the cultures were treated with 1 mM paraquate (final concentration) for 25 min (*C. jejuni* 42 °C, *A. butzleri* 30 °C, 140 rpm orbital shaking). After oxidative stress, samples were collected similarly to non-stressed cells. After 5 min incubation with RNAprotect Bacteria Reagent, bacteria were collected by centrifugation (4,700 × g, 10 min, RT). RNA was isolated by GeneJET RNA Purification Kit (Thermo Fisher Scientific; K0731) according to the manufacturer's protocol and treated with RNase-free DNase I (Thermo Fisher Scientific). Next, purification by the GeneJET RNA Purification Kit was performed to remove DNase I. A NanoDrop Lite spectrophotometer, agarose gel electrophoresis and Agilent 4200 TapeStation System were used to determine the RNA quality and quantity. RNA was isolated immediately after bacteria collection, stored at -80 °C for up to one month and used for RNA sequencing. RNA was isolated from three independent cultures.

For analyses of gene transcription dependent on oxygen supply, bacterial cells were collected from cultures under the logarithmic phase of growth (OD_{600} ~0.2-0.5), grown under the desired atmosphere (see Material and culture conditions), and RNA was isolated as described above.

RNA sequencing (RNA-seq)

Preparation and sequencing of the prokaryotic directional mRNA library were performed at the Novogene Bioinformatics Technology Co. Ltd. (Cambridge, UK). Briefly, the ribosomal RNA was removed from the total RNA, followed by ethanol precipitation. After fragmentation, the first strand of cDNA was synthesized using random hexamer primers. During the second strand cDNA synthesis, dUTPs were replaced with dTTPs in the reaction buffer. The directional library was ready after end repair, A-tailing, adapter ligation, size selection, USER enzyme digestion, amplification, and purification. The library was checked with Qubit, RT-qPCR for quantification and a bioanalyser for size distribution detection. The libraries were sequenced with the NovaSeq 6000 (Illumina), and 150 bp reads were produced.

RNA-seq analysis

The 150 bp paired reads were mapped to the *C. jejuni* NCTC 11168 (NC_002163.1) or *A. butzleri* RM4018 (NC_009850.1) genome depending on the species analyzed using Bowtie2 software with local setting (version 2.3.5.1) [70,71] and processed using samtools (version 1.10) [72], achieving more than 10^6 mapped reads on average. Differential analysis was performed using R packages Rsubread (version 2.10) and edgeR (version 3.38) [73,74], following a protocol described in [75]. Genes rarely transcribed were removed from the analysis (less than 10 mapped reads per library). The obtained count data was normalised using the edgeR package, and a quasi-likelihood negative binomial was fitted. Differential expression was tested using the glmTtreat function with a 1.45-fold change threshold. Only genes with a false discovery rate (FDR) less than 0.05 and $|\log_2 FC| \geq 1$ were considered differentially expressed. Data visualization with volcano plots was done using the EnhancedVolcano and tidyHeatmap R packages (version 1.14 and 1.8.1) [76]. The reproducibility of *C. jejuni* and *A. butzleri* biological replicates was visualized by principal component analysis (PCA) of the normalized RNA-seq CPM data (Figs S13A and S13B).

Proteomic sample preparation

Bacterial cultures of wild-type *C. jejuni* NCTC 11168 and *A. butzleri* RM4018 strains and their isogenic mutant strains, ΔCj1608 or ΔAbu0127, respectively, were grown in BHI under microaerobic conditions to OD_{600} of 0.5-0.7 and split into 2 sub-cultures of 10 ml each. The first sub-culture was harvested, washed, and lysed immediately after opening the jar; the second sub-culture (only WT strains) was harvested, washed and lysed after incubation with 1 mM paraquate (*C. jejuni*: 42 °C; *A. butzleri*: 30 °C with orbital shaking, 140 rpm) for 30 and 60 minutes. The bacterial proteomes were prepared as described previously by Abele et al. [77]. Briefly, cells were harvested by centrifugation at 10,000 × g for 2 min, media were removed, and cells were washed once with 20 ml of 1 × PBS. The cell pellets were suspended and lysed in 100 µl of 100% trifluoroacetic acid (TFA; Roth) [78] for 5 min at 55 °C. Next, 900 µl of Neutralization Buffer (2 M Tris) was added and vortexed. Protein concentration was measured using Bradford assay (Bio-Rad). 50 µg of protein per sample was reduced (9 mM TCEP) and carbamidomethylated (40 mM CAA) for 5 minutes at 95 °C. The proteins were digested by adding trypsin (proteomics grade, Roche) at a 1/50 enzyme/protein ratio (w/w) and incubation at 37 °C overnight. Digests were acidified by the addition of 3% (v/v) formic acid (FA) and desalted using self-packed StageTips (five disks per micro-column, ø 1.5 mm, C18 material, 3M Empore). The peptide eluates were dried to completeness and stored at -80 °C. Before the LC-MS/MS measurement, all samples were freshly resuspended in 12 µl 0.1% FA in HPLC grade water, and around 25 µg of total peptide amount was injected into the mass spectrometer per measurement. Each experiment was performed using four biological replicates.

Proteomic data acquisition and data analysis

Peptides were analyzed on a Vanquish Neo liquid chromatography system (micro-flow configuration) coupled to an Orbitrap Exploris 480 mass spectrometer (Thermo Fisher Scientific). Around 25 µg of peptides were applied onto an Acclaim PepMap 100 C18 column (2 µm particle size, 1 mm ID × 150 mm, 100 Å pore size; Thermo Fisher Scientific) and separated using a two-stepped gradient. In the first step, a 50-minute linear gradient ranging from 3% to 24% solvent B (0.1% FA, 3% DMSO in ACN) in solvent A (0.1% FA, 3% DMSO in HPLC grade water) at a flow rate of 50 µl/min was applied. In the second step, solvent B was further increased from 24% to 31% over a 10-minute linear gradient. The mass spectrometer was operated in data-dependent acquisition (DDA) and positive ionisation mode. MS1 full scans (360 – 1300 m/z) were acquired with a resolution of 60,000, a normalized AGC target value of 100% and a maximum injection time of 50 msec. Peptide precursor selection for fragmentation was carried out using a fixed cycle time of 1.2 sec. Only

precursors with charge states from 2 to 6 were selected, and dynamic exclusion of 30 sec was enabled. Peptide fragmentation was performed using higher energy collision-induced dissociation (HCD) and normalised collision energy of 28%. The precursor isolation window width of the quadrupole was set to 1.1 m/z. MS2 spectra were acquired with a resolution of 15,000, a fixed first mass of 100 m/z, a normalized automatic gain control (AGC) target value of 100% and a maximum injection time of 40 msec.

Peptide identification and quantification were performed using MaxQuant (version 1.6.3.4) with its built-in search engine Andromeda [79,80]. MS2 spectra were searched against the *C. jejuni or A. butzleri* proteome database derived from *C. jejuni* NCTC 11168 (NC_002163.1) or *A. butzleri* RM4018 (NC_009850.1), respectively. Trypsin/P was specified as the proteolytic enzyme. The precursor tolerance was set to 4.5 ppm, and fragment ion tolerance to 20 ppm. Results were adjusted to a 1% false discovery rate (FDR) on peptide spectrum match (PSM) level and protein level employing a target-decoy approach using reversed protein sequences. The minimal peptide length was defined as seven amino acids, carbamidomethylated cysteine was set as fixed modification and oxidation of methionine and N-terminal protein acetylation as variable modifications. The match-between-run function was disabled. Protein abundances were calculated using the Label-Free Quantification (LFQ) algorithm from MaxQuant [81]. Protein intensity values were logarithm transformed (base 2), and a Student t-test was used to identify proteins differentially expressed between conditions. The resulting p-values were adjusted by the Benjamini-Hochberg algorithm [82] to control the FDR. Since low abundant proteins are more likely to result in missing values, we filled in missing values with a constant of half the lowest detected LFQ intensity per protein. However, if the imputed value was higher than the 20% quantile of all LFQ intensities in that sample, we used the 20% quantile as the imputed value. Only proteins with $|\log_2 FC| \geq 1$ were considered differentially expressed [83].

The reproducibility of *C. jejuni* and *A. butzleri* biological replicates was visualized by principal component analysis (PCA) of the normalized LC-MS/MS CPM data (Figs S13C and S13D).

Omics data analysis

The Kyoto Encyclopedia of Genes and Genomes (KEGG) [84] gene/protein set enrichment analysis of the differentially expressed genes and proteins was performed and visualized based on the clusterProfiler [27] (version 4.8.2) package in R software with $P < 0.05$. Genome-wide functional annotation was carried out with the eggNOG-mapper (version 5.0) [85] according to the Cluster of Orthologous Genes (COGs) database [86]

with an e-value of 0.001 and minimum hit bit-score of 60. Visual representations of RNA expression levels and LC-MS/MS expressed proteins in different COGs were performed with the Circos Table viewer (http://mkweb.bcgsc.ca/tableviewer/, accessed on 05 November 2023). For the analyses, only genes and proteins with $|\log_2 FC| \geq 1$ and FDR < 0.05 were considered as significantly changed.

Chromatin immunoprecipitation (ChIP)

Bacterial cultures (70 ml BHI) of *C. jejuni* NTCT and *A. butzleri* RM4018 wild-types and ΔCj1608 and Abu0127 mutants were grown to OD_{600} of 0.5–0.7. The culture was crosslinked with 1% formaldehyde for 5 min immediately after opening the jar. The crosslinking reactions were stopped by treatment with 125 mM glycine for 10 min at room temperature. The cultures were centrifuged at 4700 × g for 10 min at 4 °C and washed twice with 25 ml of ice-cold 1 × PBS, followed by the same centrifugation step. Samples were resuspended in 1.1 ml IP buffer (150 mM NaCl, 50 mM Tris-HCl pH 7.5, 5 mM EDTA, 0.5% vol/vol NP-40, 1.0% vol/vol Triton X-100) and sonicated (Ultraschallprozessor UP200s (0.6/50% power, 30 s ON − 30 s OFF, ice bucket)) to reach 100-500 bp DNA fragment size. Next, the samples were centrifuged at 12,000 × g for 10 min at 4 °C. 100 µl of the supernatant was used for input preparation. 900 µl of the supernatant was incubated with 30 µl of Sepharose Protein A (Rockland, PA50-00-0002) (pre-equilibrated in IP buffer) for 1 h at 4 °C on a rotation wheel. The samples were centrifuged 1000 × g for 2 min at 4 °C; the supernatants were incubated with 100 µl antibody-Sepharose A complex (see below) and incubated at 4 °C for 24 h on a rotation wheel. Next, the samples were centrifuged 1000 × g for 2 min at 4 °C, and the supernatant was discarded. The beads were washed four times with IP-wash buffer (50 mM Tris-HCl pH 7.5, 150 mM NaCl, 0.5% NP-40, 0.1% SDS), twice with TE buffer (10 mM Tris-HCl, pH 8.0; 0.1 mM EDTA), resuspended in 180 µl of TE buffer, and treated with 20 µg/ml RNase A at 37 °C for 30 min. Next, crosslinks were reversed by adding SDS at a final concentration of 0.5% and proteinase K at a final concentration of 20 µg/ml, followed by incubation for 16 h at 37 °C. The beads were removed by centrifugation 1000 × g for 2 min at 4 °C, and the DNA from the supernatants were isolated with ChIP DNA Clean & Concentrator (Zymo Research). The quality of DNA was validated by electrophoresis in 2% agarose gel, and the concentration was determined with QuantiFluor dsDNA System (Promega). The ChIP-DNA was isolated from three independent bacteria cultures.

The *C. jejuni* antibody-Sepharose A complex was prepared by adding 40 µg of desalted rabbit polyclonal anti-Cj1608 antibody to 100 µl of the Sepharose Protein A pre-equilibrated in IP buffer. *A. butzleri* antibody-

sepharose A complex was prepared by adding 120 µg of desalted rabbit polyclonal anti-Abu0127 antibody to 100 µl of the Sepharose Protein A pre-equilibrated in IP buffer. The binding reaction was performed on a rotation wheel for 24 h at 4 °C. Next, the complex was washed fife times with an IP buffer. The antibodies used in ChIP were raised in rabbits under the approval of the First Local Committee for Experiments with the Use of Laboratory Animals, Wroclaw, Poland (consent number No 053/2020) and validated with Western blot (Figs S11D and S12D).

Quantitative polymerase chain reaction

RT-qPCR quantified the mRNA levels of the selected genes. The reverse transcription was conducted using 500 ng of RNA in a 20 µl volume reaction mixture of iScript cDNA Synthesis Kit (Bio-Rad). 2.5 µl of 1:10 diluted cDNA was added to 7.5 µl of Sensi-FAST SYBR No-ROX (Bioline) and 400 nM of forward and reverse primers in a 15 µl final volume. The RT-qPCR program: 95 °C for 3 min, followed by 40 three-step amplification cycles consisting of 5 s at 95 °C, 10 s at 58 °C and 20 s at 72 °C. The following primer pairs were used: P18-P19, *gltA* for *C. jejuni* RT-qPCR and P23-P24, *nuoB* for *A. butzleri* RT-qPCR (S2 Table). The relative quantity of mRNA for each gene of *C. jejuni* was determined by referring to the mRNA levels of *recA* (P25-P26 primer pair). The relative quantity of mRNA for each gene of *A. butzleri* was determined by referring to the mRNA levels of *gyrA* (P27-P28 primer pair). The RT-qPCR was performed for three independent bacterial cultures.

The protein-DNA interactions in the cell in vivo of the selected DNA regions were quantified by ChIP-qPCR. 2.5 µl of 1:10 diluted immunoprecipitation output was added to 7.5 µl of Sensi-FAST SYBR No-ROX (Bioline) and 400 nM of forward and reverse primers in a 15 µl final volume. The ChIP-qPCR was performed using the following programme: 95 °C for 3 min, followed by 40 three-step amplification cycles consisting of 10 s at 95 °C, 10 s at 59 °C and 20 s at 72 °C. The following primer pairs were used: P43-P44, p*gltA* (*C. jejuni*); P45-P46, p*nuoA* (*A. butzleri*) (S2 Table). The *recA* (P25-P26) and *gyrA* (P27-P28) genes were used as a negative control for *C. jejuni* and *A. butzleri*, respectively (S2 Table). No-antibody control was used for ChIP-qPCR normalization, and the fold enrichment was calculated. The ChIP-qPCR was performed for three independent bacterial cultures.

The RT-qPCR and ChIP-qPCR were performed using the CFX96 Touch Real-Time PCR Detection Systems, and data were analyzed with CFX Maestro (Bio-Rad) software.

Construction of plasmids expressing recombinant wild-type Cj1608 and Abu0127 proteins

The *Cj1608* (*Cj1509* in *C. jejuni* 81-116) gene (888 bp) was amplified with primer pairs P29-P30 using *C. jejuni* 81-116 genomic DNA as a template. The *Abu0127* gene (891 bp) was amplified with primer pair P31-P32 using *A. butzleri* RM4018 genomic DNA as a template. The PCR products were digested with BamHI/SalI and cloned into BamHI/SalI sites of pET28Strep[24] to generate pETStrepCj1509 and pETStrepAbu0127, respectively (S1 Table).

Protein expression and purification

The recombinant Strep-tagged Cj1608 (Cj1509 of *C. jejuni* 81-116) and Abu0127 proteins were purified according to the Strep-Tactin manufacturer's protocol (IBA Lifesciences). Briefly, *E. coli* BL21 cells (1 l) carrying either the pET28/StrepCj1509 or pET28/StrepAbu0127 vectors were grown at 37 °C. At an OD_{600} of 0.8, protein synthesis was induced with 0.05 mM IPTG for 3 hours at 30 °C for Cj1608 and overnight at 18 °C for Abu0127. The cultures were harvested by centrifugation (10 min, 5,000 × g and 4 °C). The cells were suspended in 20 ml of ice-cold buffer W (100 mM Tris-HCl, pH 8.0; 300 mM NaCl; and 1 mM EDTA) supplemented with cOmplete, EDTA-free protease inhibitor Cocktail (Roche)), disrupted by sonication, and centrifuged (30 min, 31,000 × g and 4 °C). The supernatant was applied onto a Strep-Tactin Superflow high-capacity Sepharose column (1 ml bed volume, IBA). The column was washed with buffer W until Bradford tests yielded a negative result, and then it was washed with 5 ml of buffer W without EDTA. The elution was carried out with approx. 6 × 0.8 ml of buffer E (100 mM Tris-HCl, pH 8.0; 300 mM NaCl; and 5 mM desthiobiotin). Protein purity was analyzed by SDS-PAGE electrophoresis using GelDoc XR+ and ImageLab software (BioRad). The fractions were stored at −20 °C in buffer E diluted with glycerol to a final concentration of 50%.

Electrophoretic mobility shift assay (EMSA)

PCR amplified DNA probes in two steps. DNA fragments were amplified in the first step using unlabeled primer pairs P33-P34 (p*gltA*), P35-P36 (*recJ*) with a *C. jejuni* NCTC 11168 genomic DNA template and P37-P38 (p*nuo*), P39-P40 (*recA*) with an *A. butzleri* RM4018 genomic DNA template (S1 Table). The forward primers were designed with overhangs complementary to P41 (FAM–labelled) for p*nuo* and p*gltA* and P42

(Cy5 labelled) for *recJ* and *recA*. The unlabeled fragment was purified and used as a template in the second round of PCR using the appropriate fluorophore-labelled primer and the appropriate reverse primer used in the first step. Both fluorophore-labelled DNA (each 5 nM) were incubated with the Strep-tagged protein at 30°C (Abu0127) or 37°C (Cj1608) for 20 min in Tris buffer (50 mM Tris–HCl, pH 8.0; 100 mM NaCl and 0.2% Triton X-100). The complexes were separated by electrophoresis on a 4% polyacrylamide gel in 0.5 × TBE (1 × TBE: 89 mM Tris, 89 mM borate and 2 mM EDTA) at 10 V/cm in the cold room (approx. 10 °C). The gels were analyzed using Typhoon 9500 FLA Imager and ImageQuant software.

ATP assay

The ATP level was measured with the BacTiter-Glo™ Assay. *C. jejuni and A. butzleri* cultures were grown in the BHI medium to the logarithmic growth phase (OD_{600} of 0.5-0.7). Cells were diluted to OD_{600} = 0.1 with fresh medium. Next, 50 µl of bacteria were mixed with 50 µl of BacTiter-Glo™ (Promega) and incubated at room temperature for 5 min. The luminescence was measured with a CLARIOstar® plate reader on opaque-walled multiwell plates (SPL Life Sciences; 2-200203). Each experiment was performed using three biological replicates.

Statistics and Reproducibility

Statistical analysis was performed using GraphPad Prism (8.4.2) and R (4.3.1) statistical software. All *in vivo* experiments were repeated at least three times, and data were presented as mean ± SD. The statistical significance between the two conditions was calculated by paired two-tailed Student's t-test. The statistical significance between multiple groups was calculated by one-way ANOVA with Tukey's post hoc test. $P < 0.05$ was considered statistically significant. The proteome and transcriptome correlation were determined with the Pearson correlation coefficient. The EMSA and Western blot experiments were repeated twice with similar results. Numerical data with statistics for all graphs presented in the study (S4 Data) and raw images (S1 Raw images) are provided with this paper.

Figure captions

Fig 1. RNA-seq and LC-MS/MS analyses of *C. jejuni* gene expression controlled by Cj1608. (A) The comparison of gene transcription in the *C. jejuni* wild-type (CJ), stressed wild-type (CJ_S) and Cj1608 knock-out mutant (ΔCj1608) cells revealed by RNA-seq. Genes whose transcription significantly changed ($|\log_2 FC| \geq 1$; FDR ≤ 0.05) are depicted by colored dots (see the legend in the figure). The genes named on the graph correspond to the citric acid cycle and electron transport chain. **(B)** The Venn diagram presents the number of differentially transcribed genes in the analyzed strains and conditions. **(C)** ClusterProfiler protein enrichment plot showing activation or suppression of KEGG groups in the analyzed strains. **(D)** The correlation between gene expression in ΔCj1608 and CJ cells at the transcription and proteome levels. Red dots represent homodirectional genes – up-regulated or down-regulated – at the transcriptome and proteome levels. Yellow dots represent opposite changes. Blue dots represent genes that changed only at the transcription level, while green dots represent genes that changed only at the proteome level. Numbers of differentially expressed genes in the indicated strains and conditions are given in parentheses. The proteins named on the graph correspond to the citric acid cycle and electron transport chain. **(E)** ClusterProfiler protein enrichment plot showing activation or suppression of KEGG groups in the analyzed strains. **(A, D)** Values outside the black dashed lines indicate a change in the expression of $|\log_2 FC| \geq 1$. Grey dots correspond to genes whose transcription was not significantly changed (FDR ≤ 0.05).

Fig 2. RNA-seq and LC-MS/MS analyses of *A. butzleri* gene expression controlled by Abu0127. (A) The comparison of gene transcription in the *A. butzleri* wild-type (AB), stressed wild-type (AB_S) and Abu0127 knock-out mutant (ΔAbu0127) cells revealed by RNA-seq. Genes whose transcription significantly changed ($|\log_2 FC| \geq 1$; FDR ≤ 0.05) are depicted by colored dots (see the legend in the figure). The genes named on the graph correspond to the citric acid cycle and electron transport chain. **(B)** The Venn diagram presents the number of differentially transcribed genes in the analyzed strains and conditions. **(C)** ClusterProfiler protein enrichment plot showing activation or suppression of KEGG groups in the analyzed strains. **(D)** The correlation between gene expression of ΔAbu0127 and AB cells at the transcription and proteome levels. Red dots represent homodirectional genes – up-regulated or down-regulated – at the transcriptome and proteome levels. Yellow dots represent opposite changes. Blue dots represent genes that changed only at the transcription level,

while green dots represent genes that changed only at the proteome level. Numbers of differentially expressed genes in the indicated strains and conditions are given in parentheses. The proteins named on the graph correspond to the citric acid cycle and electron transport chain. **(E)** ClusterProfiler protein enrichment plot showing activation or suppression of KEGG groups in the analyzed strains. **(A, D)** Values outside the black dashed lines indicate a change in the expression of $|\log_2 FC| \geq 1$. Grey dots correspond to genes whose transcription was not significantly changed (FDR ≤ 0.05).

Fig 3. Schematic presentation of *C. jejuni* and *A. butzleri* energy conservation factors whose expression changed in ΔCj1608 and ΔAbu0127, respectively. **(A)** Regulation of the *C. jejuni* citric acid cycle, the selected associated catabolic pathways, and nutrient transporters. **(B)** Regulation of *C. jejuni* electron transport chain enzymes. **(C)** Regulation of the *A. butzleri* tricarboxylic acid cycle selected associated catabolic pathways and nutrient transporters. **(D)** Regulation of *A. butlzeri* electron transport chain enzymes. **(A-D)** The increase or decrease in protein abundance in the deletion mutant strains compared to wild-type strains is shown based on the LC-MS/MS data (S3 Data). When MS did not detect the protein, but the corresponding transcript level was increased or decreased, the color code depicts RNA-seq results (denoted as □). For details concerning transcriptomic data or complex transcriptome/proteome interpretation (denoted as *). Frd, fumarate reductases; Hyd, Hya, Hua, hydrogenases, Lut, Dld, L-lactate utilization complex, Fdh, formate dehydrogenase; Mqo, malate:quinone oxidoreductase, Nuo, NADH-quinone oxidoreductase; Nrf, nitrate reductase; Tor, SN oxide reductase; Nap, nitrate reductase; Mfr, methylmenaquinol:fumarate reductase (misannotated as succinate dehydrogenase Sdh); SOR, sulfite:cytochrome c oxidoreductase; Cio, cyanide-insensitive cytochrome bd-like quinol oxidase; Cco, cbb3-type cytochrome c oxidase; Pet, ubiquinol-cytochrome C reductase; Gdh, gluconate 2-dehydrogenase; SOX, thiosulfate oxidation by SOX system; Oor, 2-oxoglutarate:acceptor oxidoreductase; POR, pyruvate:acceptor oxidoreductase; PEP, phosphoeneoopyruvate; G-6Pglucose 6-phosphate.; "?" unknown enzyme. All genes and enzyme complexes can be found in S3 Data.

Fig 4. Impact of Cj1608 and Abu0127 on gene regulation in *C. jejuni* and *A. butzleri*, respectively. **(A)** Circos plots presenting the correlation between Cluster of Orthologues Group (COG) and differentially

expressed *C. jejuni* genes revealed by RNA-seq in the ΔCj1608 strain compared to the *C. jejuni* wild-type strain. **(B)** Circos plots presenting the correlation between COG and differentially expressed *A. butzleri* genes revealed by RNA-seq in the ΔAbu0127 strain compared to the *A. butzleri* wild-type strain. **(C)** Circos plots presenting the correlation between COG and differentially expressed *C. jejuni* proteins revealed by LC-MS/MS in the ΔCj1608 strain compared to the *C. jejuni* wild-type strain. **(D)** Circos plots presenting the correlation between COG and differentially expressed *A. butzleri* proteins revealed by LC-MS/MS in the ΔAbu0127 strain compared to the *A. butzleri* wild-type strain. **(A-D)** Expression changes of $\log_2 FC| \geq 1$ and FDR ≥ 0.05 were considered significant and included in the analyses. The category of unknown genes was excluded from the analysis.

Fig 5. Cj1608-dependent control of *C. jejuni* energy conservation pathways. (A) Growth curves and generation times (G) of *C. jejuni* wild-type (CJ),Cj1608 knock-out mutant (ΔCj1608) and Cj1608 complementation (C_{Cj1608}) strains cultivated in the presence of H_2 or without H_2; G, generation time; ND, non-determined. **(B),** ATP production by CJ,ΔCj1608 and C_{Cj1608} strains cultivated as in part A. **(C)** ChIP-qPCR analysis of p*gltA* fragment immunoprecipitated from CJ and ΔCj1608 cultured under microaerobic conditions. The *recA* gene was used as a negative control which Cj1608 does not bind. **(D)** EMSA analysis of Cj1608 binding to the p*gltA*-FAM promoter region *in vitro*. The *recA*-Cy5 fragment was used as a negative control. **(E)** RT-qPCR analysis of *gltA* transcription in CJ,ΔCj1608 and C_{Cj1608} cells cultured at different oxygen concentrations: (i) 1% O_2, (ii) 5% O_2, or (iii) 10% O_2 (see Materials and Methods). **(F)** Growth curves of CJ,ΔCj1608 and C_{Cj1608} strains cultivated as in part E. **(G)** ATP production by CJ,ΔCj1608 and C_{Cj1608} strains cultivated as in part E**. (A-C, E-G),** Data presented as the mean values ± SD. Ordinary one-way ANOVA with Tukey's multiple comparison test determined the P value. n = 3 biologically independent experiments.

Fig 6. Abu0127-dependent control of *A. butzleri* energy conservation pathways. (A) Growth curves and generation times (G) of *A. butzleri* wild-type (AB) and Abu0127 knock-out mutant (ΔAbu0127) strains cultivated in the presence of H_2 or without H_2; G, generation time. **(B)** ATP production by AB and ΔAbu0127 strains cultivated as in part A. **(C)** ChIP fold enrichment of DNA fragment in p*nuoA-N* by ChIP-qPCR in AB and ΔAbu0127 cultured under microaerobic conditions. The *gyrA* gene was used as a negative control not

bound by Abu0127. **(D)** EMSA analysis of Abu0127 binding to the p*nuoA*-FAM promoter region *in vitro*. The *recJ*-Cy5 fragment was used as a negative control. **(E)** RT-qPCR analysis of *nuoB* transcription in AB and ΔAbu0127 strains cultured at different oxygen concentrations: (i) 1% O_2; (ii) 5% O_2 or (iii) 10% O_2 (see Materials and Methods). **(F)** Growth curves of AB and ΔAbu0127 strains cultivated as in part E. **(G)** ATP production by AB and ΔAbu0127 strains cultivated as in part E. **(A-C, E-G)** Data presented as the mean values ± SD. Ordinary one-way ANOVA with Tukey's multiple comparison test determined the P value. n = 3 biologically independent experiments.

Supporting information

S1 Fig. Disc diffusion assay of *C. jejuni* and *A. butzleri* indicating the influence of Cj1608 and Abu0127 on resistance to oxidative agents. (A) *C. jejuni* wild-type (CJ)), Cj1608 knock-out mutant (ΔCj1608) and Cj1608 complementation (C_{Cj1608}),and **(B)** *A. butzleri* wild-type (AB) and Abu0127 knock-out mutant (ΔAbu0127) strains were analyzed. The black dashed lines indicate the disc size. Data have been depicted as the mean values ± SD. n = 3 biologically independent experiments. **(A)** Ordinary one-way ANOVA with Tukey's multiple comparison test determined the P value. **(B)** The students' paired t-test determined the P value. Data taken from [33].

S2 Fig. RNA-seq analysis of *C. jejuni* gene transcription controlled by Cj1608. (A) The Volcano plot of genes differently transcribed in the Cj1608 knock-out mutant (ΔCj1608) strain compared to the *C. jejuni* wild-type (CJ) strain (ΔCj1608-CJ). **(B)** The Volcano plot of genes differently transcribed in the CJ strain under oxidative stress induced by 1 mM paraquat (CJ_S) compared to the non-stressed wild-type strain (CJ_S-CJ). **(C)** Volcano plot of genes differently transcribed in the ΔCj1608 strain under oxidative stress induced by 1 mM paraquat ($\Delta Cj1608_S$) compared to the non-stressed ΔCj1608 mutant ($\Delta Cj1608_S$-ΔCj1608). **(D)** The comparison of gene transcription in the *C. jejuni* CJ, CJ_S, ΔCj1608 and stressed $\Delta Cj1608_S$ cells revealed by RNA-seq. The genes signed on the graph correspond to the citric acid cycle and electron transport chain. **(A-D)** Values outside the black dashed lines indicate a change in the expression of $|\log_2 FC| \geq 1$. Grey dots correspond to genes whose transcription was not significantly changed (FDR ≤ 0.05). Genes whose transcription significantly changed ($|\log_2 FC| \geq 1$; FDR ≤ 0.05) are depicted by colored dots; see the legend in the figure.

S3 Fig. RNA-seq analysis of *A. butzleri* gene transcription controlled by Abu0127. (A) The Volcano plot of genes differently transcribed in the Abu0127 knock-out mutant (ΔAbu0127) strain compared to the *A. butzleri* wild-type (AB) strain(ΔAbu0127-AB). **(B)** The Volcano plot of genes differently transcribed in the AB strain under oxidative stress induced by 1 mM paraquat (AB_S) compared to the non-stressed wild-type strain (AB_S-AB). **(C)** Volcano plot of genes differently transcribed in the ΔAbu0127 strain under oxidative stress induced by 1 mM paraquat ($\Delta Abu0127_S$) compared to the non-stressed ΔAbu0127 mutant ($\Delta Abu0127_S$-ΔAbu0127). **(D)** The comparison of gene transcription in the *A. butzleri* AB, AB_S, ΔAbu0127 and stressed $\Delta Abu0127_S$ cells revealed by RNA-seq. The genes signed on the graph correspond to the citric acid cycle and

electron transport chain. **(A-D)** Values outside the black dashed lines indicate a change in the expression of $|\log_2 FC| \geq 1$. Grey dots correspond to genes whose transcription was not significantly changed (FDR ≤ 0.05). Genes whose transcription significantly changed ($|\log_2 FC| \geq 1$; FDR ≤ 0.05) are depicted by colored dots; see the legend in the figure.

S4 Fig. LC-MS/MS analysis of *C. jejuni* and *A. butzleri* protein level regulation mediated by Cj1608 and Abu0127, respectively. (A) Volcano plot of proteins differently expressed in the Cj1608 knock-out mutant (ΔCj1608) strain compared to the *C. jejuni* wild-type (CJ) strain (ΔCj1608-CJ). **(B)** Volcano plot of proteins differentially expressed in the CJ strain after 30-min oxidative stress (CJ_S30) induced by 1 mM paraquat compared to the non-stressed wild-type strain (CJ_S30-CJ). **(C)** Volcano plot of proteins differentially expressed in the CJ strain after 60 min of oxidative stress (CJ_S60) induced by 1 mM paraquat compared to the non-stressed CJ strain (CJ_S60-CJ). **(D)** Volcano plot of proteins differently expressed in the Abu0127 knock-out mutant (ΔAbu0127)strain compared to the *A. butzleri* wild-type (AB) strain (ΔAbu0127-AB). **(E)** Volcano plot of proteins differentially expressed in the AB strain after 30-min oxidative stress (AB_S30) induced by 1 mM paraquat compared to the non-stressed AB strain (AB_S30-AB). **(F)** Volcano plot of proteins differentially expressed in the AB strain after 60 min of oxidative stress (AB_S60) induced by 1 mM paraquat compared to the non-stressed AB strain (AB_S60-AB). **(A-F)** n = 4 biologically independent experiments. Green dots correspond to genes with $|\log_2 FC| \geq 1$ and FDR ≥ 0.05; blue dots correspond to genes with $|\log_2 FC| \leq 1$ and FDR ≤ 0.05; red dots correspond to genes with $|\log_2 FC| \geq 1$ and FDR ≤ 0.05; grey dots correspond to genes that were not significantly changed. NS, non-significant. FDR, false discovery rate.

S5 Fig. Pearson correlation analysis between proteomics and transcriptomics data of (A) *C. jejuni* and (B) *A. butzleri*. Scatter plots of the correlation between data sets of the $\log_2 FC$ of gene transcript (x-axis) and proteome (y-axis) of ΔCj1608-CJ and ΔAbu0127-AB, respectively. The red line represents the regression line; r, Pearson correlation coefficient.

S6 Fig. The KEGG pathway enrichment of *C. jejuni* citrate cycle. (A) Gene enrichment of the citrate cycle KEGG group visualized by ClusterProfiler. Gene expression values are mapped to a gradient color scale of

log_2FC. **(B)** Protein enrichment of the citrate cycle KEGG group visualised by ClusterProfiler. Protein expression values are mapped to a gradient color scale of log_2FC.

S7 Fig. The KEGG pathway enrichment of *A. butzleri* oxidative phosphorylation and citrate cycle. (A) Gene enrichment of oxidative phosphorylation KEGG group visualized by ClusterProfiler. Gene expression values are mapped to a gradient colour scale of log_2FC. **(B)** Protein enrichment of oxidative phosphorylation KEGG group visualized by ClusterProfiler. Protein expression values are mapped to a gradient colour scale of log_2FC. **(C)** Gene enrichment of the citrate cycle KEGG group visualized by ClusterProfiler. Protein expression values are mapped to a gradient color scale of log_2FC.

S8 Fig. Transcriptomics and proteomics data of citrate synthetase operon. (A) RNA-seq data profile comparing *gltA* transcription in *C. jejuni* wild-type (CJ), Cj1608 knock-out mutant (ΔCj1608) strains under microaerobic growth and paraquat-induced oxidative stress. Values above the black dashed lines indicate a change in the expression of $|log_2FC| \geq 1$; FDR ≤ 0.05. **(B)** Logarithmically transformed LFQ intensities of GltA protein in CJ and ΔCj1608 strains. The student's unpaired t-test determined the P value. n = 4 biologically independent experiments. **(C)** RT-qPCR analysis of *gltA* transcription in CJ,ΔCj1608 and Cj1608 complementation (C_{Cj1608}) strains cells cultured under microaerobic or paraquat-induced oxidative stress conditions. n = 3 biologically independent experiments. Data presented as the mean values ± SD. Ordinary one-way ANOVA with Tukey's multiple comparison test determined the P value.

S9 Fig. Transcriptomics and proteomics data of NADH-quinone oxidoreductase operon. (A) RNA-seq data profile comparing the transcription of the *nuo* operon in *A. butzleri* wild-type (AB) and Abu0127 knock-out mutant (ΔAbu0127)strains under microaerobic growth and paraquat-induced oxidative stress Values above the black dashed lines indicate a change in the expression of $|log_2FC| \geq 1$; FDR ≤ 0.05. **(B)** Logarithmically transformed LFQ intensities of Nuo B-F, GltA, NuoG, and NuoI proteins in AB and ΔAbu0127 strains. n = 4 biologically independent experiments. **(C)** RT-qPCR analysis of *nuoB* transcription in AB and ΔAbu0127 cells cultured under microaerobic or paraquat-induced oxidative stress conditions. **(B and C)** Data presented as the mean values ± SD. Ordinary one-way ANOVA with Tukey's multiple comparison test determined the P value. n = 3 biologically independent experiments.

S10 Fig. Impact of HP1021 on gene regulation in *H. pylori*. (A) Circos plots presenting the correlation between Cluster of Orthologues Group (COG) and differentially expressed *H. pylori* genes revealed by RNA-seq ($|\log_2 FC| \geq 1$ and FDR ≥ 0.05) in the HP1021 knock-out mutant (ΔHP1021) strain compared to the *H. pylori* wild-type strain. **(B)** Circos plots presenting the correlation between COG and differentially expressed *H. pylori* proteins revealed by LC-MS/MS ($|\log_2 FC| \geq 1$ and FDR ≥ 0.05) in the ΔHP1021 strain compared to the *H. pylori* wild-type strain. **(C)** ClusterProfiler gene enrichment plot showing suppression of KEGG groups revealed by RNA-seq in the ΔHP1021 strain compared to the *H. pylori* wild-type strain. **(D)** Gene enrichment of citrate cycle KEGG group visualized by ClusterProfiler. Gene expression values are mapped to a gradient color scale of $\log_2 FC$. **(A-D)** Data prepared based on [26].

S11 Fig. *C. jejuni* NCTC 11168 ΔCj1608 knock-out mutant construction. (A) The mutagenesis strategy used to delete and subsequently complement Cj1608 on the *C. jejuni* chromosome. For the plasmids and primer sequences, see S1 Table and S2 Table, respectively. **(B)** RNA-seq data profile of Cj1608 gene of *C. jejuni* wild-type (CJ) and ΔCj1608 strains with the expression comparison. **(C)** Western blot analysis of Cj1608 in CJ and ΔCj1608 and complementation (C_{Cj1608}) strains. Lysate of each strain was resolved in a 10% SDS-PAGE gel and visualized by the TCE-UV method. **(D)** Cj1608 was detected in bacterial lysates by a rabbit polyclonal anti-StrepCj1608 antibody. M, PageRuler Prestained Protein Ladder (Thermo Fisher Scientific). Digital processing was applied equally across the entire image.

S12 Fig. *A. butzleri* RM4018 ΔAbu0127 knock-out mutant construction. (A) The mutagenesis strategy used to delete Abu0127 on the *A. butzleri* chromosome. For the plasmids and primer sequences, see S1 Table and S2 Table, respectively. **(B)** RNA-seq data profile of Abu0127 gene in *A. butzleri* wild-type (AB) and ΔAbu0127 strains with the expression comparison. **(C)** Western blot analysis of Abu0127 in AB and ΔAbu0127strains. Lysate of each strain was resolved in a 12% SDS-PAGE gel and visualized by the TCE-UV method. 2.5 ng of StrepAbu0127 was used as a positive control. **(D)** Abu0127 and StrepAbu0127 were detected by a rabbit polyclonal anti-StrepAbu0127 antibody. M, PageRuler Prestained Protein Ladder (Thermo Fisher Scientific). Digital processing was applied equally across the entire image.

S13 Fig. The reproducibility of *C. jejuni* and *A. butzleri* biological replicates in omics data. (A) Principal component analysis (PCA) of the normalized RNA-seq CPM data of *C. jejuni* wild-type (CJ) and Cj1608 knock-out mutant (ΔCj1608) strains under microaerobic and paraquat-induced oxidative stress conditions (CJ_S and $\Delta Cj1608_S$). **(B)** PCA of the normalized LC-MS/MS CPM data of CJ and ΔCj1608 strains under microaerobic conditions. **(C)** PCA of the normalized RNA-seq CPM data of *A. butzleri* wild-type (AB) and Abu0127 knock-out mutant (ΔAbu1027) strains under microaerobic and paraquat-induced oxidative stress conditions (AB_S and $\Delta Abu0127_S$). **(D)** PCA of the normalized proteomics CPM data of AB and ΔAbu1027 strains under microaerobic conditions.

S1 Table. Strains, plasmids, and proteins used in this study.

S2 Table. Primers used in this study.

S1 Data. Analysis of Cj1608-dependent gene expression in *C. jejuni* WT and Cj1608 knock-out mutant (ΔCj1608) strains under microaerobic and oxidative stress conditions. RNA-seq and LC-MS/MS data are presented. Genes are annotated according to the *C. jejuni* NCTC 11168 strain (NC_002163.1).

S2 Data. Analysis of Abu0127-dependent gene expression in *A. butzleri* WT and Abu0127 knock-out mutant (ΔAbu0127) strains under microaerobic and oxidative stress conditions. RNA-seq and LC-MS/MS data are presented. Genes are annotated according to the *A. butzleri* RM4018 strain (NC_009850.1).

S3 Data. Comprehensive RNA-seq and LC-MS/MS data results for genes of selected processes or pathways in *C. jejuni* and *A. butzleri*. Part of the data was compared to *H. pylori* omics data from [26]. Transcriptomic and proteomic data are presented as log_2-fold changes. Legends specific to each pathway/process were added below particular tables.

S4 Data. Numerical data with statistics for all graphs presented in the study.

S1 Raw images. Uncropped EMSA gels and Western blots.

Acknowledgements

We thank Kinga Surmacz for helping with disc diffusion assays, Maria Cieślak for helping with pUC18/ΔAbu0127 plasmid preparation, and Verena Breitner and Tayma Midari for technical assistance at BayBioMS.

Author Contributions

Conceptualization: Mateusz Noszka, Kerstin Stingl, Anna Zawilak-Pawlik

Investigation: Mateusz Noszka, Jakub Muraszko, Miriam Abele, Kerstin Stingl

Data curation: Mateusz Noszka, Agnieszka Strzałka, Miriam Abele, Christina Ludwig, Anna Zawilak-Pawlik

Formal analysis: Mateusz Noszka, Agnieszka Strzałka, Dirk Hofreuter, Miriam Abele, Christina Ludwig, Anna Zawilak-Pawlik

Software: Mateusz Noszka, Agnieszka Strzałka

Visualization: Mateusz Noszka, Agnieszka Strzałka, Anna Zawilak-Pawlik

Funding acquisition: Christina Ludwig, Anna Zawilak-Pawlik

Supervision: Anna Zawilak-Pawlik

Writing – original draft: Mateusz Noszka, Anna Zawilak-Pawlik

Writing – review & editing: Mateusz Noszka, Jakub Muraszko, Agnieszka Strzałka, Dirk Hofreuter, Miriam Abele, Christina Ludwig, Kerstin Stingl, Anna Zawilak-Pawlik

Data Availability

The *C. jejuni* RNA-seq FASTQ and processed data generated in this study have been deposited in the ArrayExpress database (EMBL-EBI) under accession code E-MTAB-13650 (https://www.ebi.ac.uk/biostudies/arrayexpress/studies/E-MTAB-13650?key=f68add96-f3b8-4030-84e6-6bcaf7b516de).

The *A. butzleri* RNA-seq FASTQ and processed data generated in this study have been deposited in the ArrayExpress database (EMBL-EBI) under accession code E-MTAB-13649 (https://www.ebi.ac.uk/biostudies/arrayexpress/studies/E-MTAB-13649?key=1f9e4a2b-4410-4d0d-b278-471d6bbf4e2e).

The raw proteomics data, MaxQuant search results, and the used protein sequence database generated in this study have been deposited in the ProteomeXchange Consortium via the PRIDE partner repository [87] under accession code PXD048711 (https://proteomecentral.proteomexchange.org/cgi/GetDataset?ID=PXD048711, reviewer account username: reviewer_pxd048711@ebi.ac.uk, password: qA73ZPq3).

Campylobacter jejuni NCTC 11168 reference genome is deposited in the National Center for Biotechnology Information under accession code NC_002163.1 (https://www.ncbi.nlm.nih.gov/nuccore/NC_002163.1).

Arcobacter butzleri RM4018 reference genome is deposited in the National Center for Biotechnology Information under accession code NC_009850.1 (https://www.ncbi.nlm.nih.gov/nuccore/NC_009850).

All of the code and data used to generate the figures presented here are deposited in GitHub via https://github.com/NoszkaM/LBMM.git.

Funding

This work has been supported by the OPUS 17, Project Number 2019/33/B/NZ6/01648, founded by the National Science Centre, Poland, to Anna Zawilak-Pawlik.

This work has been supported by the EPIC-XS, Project Number 823839, funded by the Horizon 2020 Program of the European Union, to Christina Ludwig.

Competing interests

The authors have declared that no competing interests exist.

Abbreviations

aa, amino acid; *oriC*, origin of replication; AGC, automatic gain control; BHI, Brain Heart Infusion Broth; CAA, carbamidomethylated; CemR, *Campylobacterial* energy and metabolism regulators; ChIP, chromatin immunoprecipitation; COG, Clusters of Orthologous Groups; ETC, electron transport chain; G, generation time; DDA, data-dependent acquisition; ECFσ, extracytoplasmic sigma factors; EMSA, electrophoretic mobility shift assay; FA, formic acid; FDR, false discovery rate; HCD, collision-induced dissociation; KEGG, Kyoto Encyclopedia of Genes and Genomes; LC-MS, Liquid chromatography-mass spectrometry LFQ, Label-Free Quantification MuGENT, Multiplex Genome Editing by Natural Transformation; OD, optical density; PCA, principal component analysis; PMF, proton motive force; PSM, peptide spectrum match; RNA-seq, RNA sequencing; ROS, reactive oxygen species; TCA, tricarboxylic acid cycle; TFA, trifluoroacetic acid.

References

1. Waite DW, Chuvochina MS, Hugenholtz P. Road Map of the Phylum Campylobacterota. Bergey's Man Syst Archaea Bact. 2019; 1–11. doi:10.1002/9781118960608.BM00040
2. Chieffi D, Fanelli F, Fusco V. Arcobacter butzleri: Up-to-date taxonomy, ecology, and pathogenicity of an emerging pathogen. Compr Rev food Sci food Saf. 2020;19: 2071–2109. doi:10.1111/1541-4337.12577
3. Burnham PM, Hendrixson DR. Campylobacter jejuni: collective components promoting a successful enteric lifestyle. Nat Rev Microbiol 2018 169. 2018;16: 551–565. doi:10.1038/s41579-018-0037-9
4. Shange N, Gouws P, Hoffman LC. Campylobacter and Arcobacter species in food-producing animals: prevalence at primary production and during slaughter. World J Microbiol Biotechnol 2019 359. 2019;35: 1–16. doi:10.1007/S11274-019-2722-X
5. Tacconelli E, Carrara E, Savoldi A, Harbarth S, Mendelson M, Monnet DL, et al. Discovery, research, and development of new antibiotics: the WHO priority list of antibiotic-resistant bacteria and tuberculosis. Lancet Infect Dis. 2018;18: 318–327. doi:10.1016/S1473-3099(17)30753-3
6. Sciortino S, Arculeo P, Alio V, Cardamone C, Nicastro L, Arculeo M, et al. Occurrence and Antimicrobial Resistance of Arcobacter spp. Recovered from Aquatic Environments. Antibiot 2021, Vol 10, Page 288. 2021;10: 288. doi:10.3390/ANTIBIOTICS10030288
7. Gumerov VM, Ulric LE, Or I, Zhulin B. MiST 4.0: a new release of the microbial signal transduction database, now with a metagenomic component. Nucleic Acids Res. 2023;2023: 1–7. doi:10.1093/NAR/GKAD847
8. Gundogdu O, Bentley SD, Holden MT, Parkhill J, Dorrell N, Wren BW. Re-annotation and re-analysis of the Campylobacter jejuni NCTC11168 genome sequence. BMC Genomics. 2007;8: 1–8. doi:10.1186/1471-2164-8-162/TABLES/4
9. Miller WG, Parker CT, Rubenfield M, Mendz GL, Wösten MMSM, Ussery DW, et al. The Complete Genome Sequence and Analysis of the Epsilonproteobacterium Arcobacter butzleri. PLoS One. 2007;2. doi:10.1371/JOURNAL.PONE.0001358
10. Martinez-Malaxetxebarria I, Muts R, van Dijk L, Parker CT, Miller WG, Huynh S, et al. Regulation of Energy Metabolism by the Extracytoplasmic Function (ECF) σ Factors of Arcobacter butzleri. PLoS One. 2012;7: e44796. doi:10.1371/JOURNAL.PONE.0044796
11. Gahamanyi N, Song DG, Mboera LEG, Matee MI, Mutangana D, Amachawadi RG, et al. Insights into the Virulence of Campylobacter jejuni Associated with Two-Component Signal Transduction Systems and Single Regulators. Microbiol Res 2022, Vol 13, Pages 188-200. 2022;13: 188–200. doi:10.3390/MICROBIOLRES13020016
12. Chandrashekhar K, Kassem II, Rajashekara G. Campylobacter jejuni transducer like proteins: Chemotaxis and beyond. Gut Microbes. 2017;8: 323. doi:10.1080/19490976.2017.1279380
13. Casado J, Lanas Á, González A. Two-component regulatory systems in Helicobacter pylori and Campylobacter jejuni: Attractive targets for novel antibacterial drugs. Front Cell Infect Microbiol. 2022;12: 977944. doi:10.3389/FCIMB.2022.977944/BIBTEX
14. Taylor AJ, Kelly DJ. The function, biogenesis and regulation of the electron transport chains in Campylobacter jejuni: New insights into the bioenergetics of a major food-borne pathogen. Adv Microb Physiol. 2019;74: 239–329. doi:10.1016/BS.AMPBS.2019.02.003
15. Flint A, Stintzi A, Saraiva LM. Oxidative and nitrosative stress defences of Helicobacter and Campylobacter species that counteract mammalian immunity. FEMS Microbiol Rev. 2016;40: 938–960. doi:10.1093/FEMSRE/FUW025
16. Shan Y, Lai Y, Yan A. Metabolic reprogramming under microaerobic and anaerobic conditions in bacteria. Subcell Biochem. 2012;64: 159–179. doi:10.1007/978-94-007-5055-5_8/FIGURES/4
17. Imlay JA. Where in the world do bacteria experience oxidative stress? Environ Microbiol. 2019;21: 521. doi:10.1111/1462-2920.14445
18. Espey MG. Role of oxygen gradients in shaping redox relationships between the human intestine and its microbiota. Free Radic Biol Med. 2013;55: 130–140. doi:10.1016/J.FREERADBIOMED.2012.10.554
19. van der Stel AX, van de Lest CHA, Huynh S, Parker CT, van Putten JPM, Wösten MMSM. Catabolite repression in Campylobacter jejuni correlates with intracellular succinate levels. Environ Microbiol. 2018;20: 1374–1388. doi:10.1111/1462-2920.14042
20. van der Stel A-X, Wösten MMSM. Regulation of Respiratory Pathways in Campylobacterota: A

Review. Front Microbiol. 2019;10: 424488. doi:10.3389/FMICB.2019.01719

21. Ravcheev DA, Gerasimova A V., Mironov AA, Gelfand MS. Comparative genomic analysis of regulation of anaerobic respiration in ten genomes from three families of gamma-proteobacteria (Enterobacteriaceae, Pasteurellaceae, Vibrionaceae). BMC Genomics. 2007;8: 1–17. doi:10.1186/1471-2164-8-54/FIGURES/5

22. Tomb JF, White O, Kerlavage AR, Clayton RA, Sutton GG, Fleischmann RD, et al. The complete genome sequence of the gastric pathogen Helicobacter pylori. Nature. 1997;388: 539–547. doi:10.1038/41483

23. Donczew R, Makowski L, Jaworski P, Bezulska M, Nowaczyk M, Zakrzewska-Czerwińska J, et al. The atypical response regulator HP1021 controls formation of the Helicobacter pylori replication initiation complex. Mol Microbiol. 2015;95: 297–312. doi:10.1111/MMI.12866/SUPPINFO

24. Szczepanowski P, Noszka M, Zdot;yła-Uklejewicz D, Pikuła F, Nowaczyk-Cieszewska M, Krężel A, et al. HP1021 is a redox switch protein identified in Helicobacter pylori. Nucleic Acids Res. 2021;49: 6863–6879. doi:10.1093/NAR/GKAB440

25. Pflock M, Bathon M, Schär J, Müller S, Mollenkopf H, Meyer TF, et al. The Orphan Response Regulator HP1021 of Helicobacter pylori Regulates Transcription of a Gene Cluster Presumably Involved in Acetone Metabolism. J Bacteriol. 2007;189: 2339. doi:10.1128/JB.01827-06

26. Noszka M, Strzałka A, Muraszko J, Kolenda R, Meng C, Ludwig C, et al. Profiling of the Helicobacter pylori redox switch HP1021 regulon using a multi-omics approach. Nat Commun 2023 141. 2023;14: 1–14. doi:10.1038/s41467-023-42364-6

27. Wu T, Hu E, Xu S, Chen M, Guo P, Dai Z, et al. clusterProfiler 4.0: A universal enrichment tool for interpreting omics data. Innovation. 2021;2. doi:10.1016/j.xinn.2021.100141

28. Li S, Lam J, Souliotis L, Alam MT, Constantinidou C. Posttranscriptional Regulation in Response to Different Environmental Stresses in Campylobacter jejuni. Microbiol Spectr. 2022;10. doi:10.1128/SPECTRUM.00203-22/SUPPL_FILE/REVIEWER-COMMENTS.PDF

29. Sharma CM, Hoffmann S, Darfeuille F, Reignier J, Findeiß S, Sittka A, et al. The primary transcriptome of the major human pathogen Helicobacter pylori. Nat 2010 4647286. 2010;464: 250–255. doi:10.1038/nature08756

30. Flint A, Stintzi A. Cj1386, an Atypical Hemin-Binding Protein, Mediates Hemin Trafficking to KatA in Campylobacter jejuni. J Bacteriol. 2015;197: 1002. doi:10.1128/JB.02346-14

31. Fasnacht M, Polacek N. Oxidative Stress in Bacteria and the Central Dogma of Molecular Biology. Front Mol Biosci. 2021;8: 392. doi:10.3389/FMOLB.2021.671037/BIBTEX

32. Stahl M, Butcher J, Stintzi A. Nutrient Acquisition and Metabolism by Campylobacter jejuni. Front Cell Infect Microbiol. 2012;2: 5. doi:10.3389/FCIMB.2012.00005

33. Surmacz K. Analysis of Aliarcobacter butzleri RM4018 sensitivity to oxidative stress. Wroclaw University of Science and Technology. 2022.

34. Zhu M, Dai X. Maintenance of translational elongation rate underlies the survival of Escherichia coli during oxidative stress. Nucleic Acids Res. 2019;47: 7592–7604. doi:10.1093/NAR/GKZ467

35. Benoit SL, Maier RJ, Sawers RG, Greening C. Molecular Hydrogen Metabolism: a Widespread Trait of Pathogenic Bacteria and Protists. Microbiol Mol Biol Rev. 2020;84. doi:10.1128/MMBR.00092-19/ASSET/A83CAA42-57CA-4332-9E92-AACC8CBE45E4/ASSETS/GRAPHIC/MMBR.00092-19-F0008.JPEG

36. Guccione EJ, Kendall JJ, Hitchcock A, Garg N, White MA, Mulholland F, et al. Transcriptome and proteome dynamics in chemostat culture reveal how Campylobacter jejuni modulates metabolism, stress responses and virulence factors upon changes in oxygen availability. Environ Microbiol. 2017;19: 4326. doi:10.1111/1462-2920.13930

37. Kiehlbauch JA, Brenner DJ, Nicholson MA, Baker CN, Patton CM, Steigerwalt AG, et al. Campylobacter butzleri sp. nov. isolated from humans and animals with diarrheal illness. J Clin Microbiol. 1991;29: 376. doi:10.1128/JCM.29.2.376-385.1991

38. Ward B. Bacterial Energy Metabolism. Mol Med Microbiol. 2015; 201–233. doi:10.1016/B978-0-12-397169-2.00011-1

39. Perez JC, Groisman EA. Evolution of transcriptional regulatory circuits in bacteria. Cell. 2009;138: 233. doi:10.1016/J.CELL.2009.07.002

40. Federowicz S, Kim D, Ebrahim A, Lerman J, Nagarajan H, Cho B kwan, et al. Determining the control circuitry of redox metabolism at the genome-scale. PLoS Genet. 2014;10. doi:10.1371/JOURNAL.PGEN.1004264

41. Myers KS, Yan H, Ong IM, Chung D, Liang K, Tran F, et al. Genome-scale Analysis of Escherichia

coli FNR Reveals Complex Features of Transcription Factor Binding. PLOS Genet. 2013;9: e1003565. doi:10.1371/JOURNAL.PGEN.1003565

42. Brown AN, Anderson MT, Bachman MA, Mobley HLT. The ArcAB Two-Component System: Function in Metabolism, Redox Control, and Infection. Microbiol Mol Biol Rev. 2022;86. doi:10.1128/MMBR.00110-21/ASSET/108E9BE2-5A15-4E52-B25B-B064F8CBF879/ASSETS/IMAGES/LARGE/MMBR.00110-21-F004.JPG

43. Park DM, Akhtar MS, Ansari AZ, Landick R, Kiley PJ. The bacterial response regulator ArcA uses a diverse binding site architecture to regulate carbon oxidation globally. PLoS Genet. 2013;9. doi:10.1371/JOURNAL.PGEN.1003839

44. Stewart V. Dual interacting two-component regulatory systems mediate nitrate- and nitrite-regulated gene expression in Escherichia coli. Res Microbiol. 1994;145: 450–454. doi:10.1016/0923-2508(94)90093-0

45. Iyer MS, Pal A, Srinivasan S, Somvanshi PR, Venkatesh K V. Global Transcriptional Regulators Fine-Tune the Translational and Metabolic Efficiency for Optimal Growth of Escherichia coli. mSystems. 2021;6. doi:10.1128/MSYSTEMS.00001-21

46. Overton TW, Griffiths L, Patel MD, Hobman JL, Penn CW, Cole JA, et al. Microarray analysis of gene regulation by oxygen, nitrate, nitrite, FNR, NarL and NarP during anaerobic growth of Escherichia coli: new insights into microbial physiology. Biochem Soc Trans. 2006;34: 104–107. doi:10.1042/BST0340104

47. Unden G, Bongaerts J. Alternative respiratory pathways of Escherichia coli: energetics and transcriptional regulation in response to electron acceptors. Biochim Biophys Acta. 1997;1320: 217–234. doi:10.1016/S0005-2728(97)00034-0

48. van der Stel AX, van Mourik A, Heijmen-van Dijk L, Parker CT, Kelly DJ, van de Lest CHA, et al. The Campylobacter jejuniRacRS system regulates fumarate utilization in a low oxygen environment. Environ Microbiol. 2015;17: 1049–1064. doi:10.1111/1462-2920.12476/SUPPINFO

49. Liu X, Gao B, Novik V, Galán JE. Quantitative Proteomics of Intracellular Campylobacter jejuni Reveals Metabolic Reprogramming. PLoS Pathog. 2012;8. doi:10.1371/JOURNAL.PPAT.1002562

50. Galperin MY. A census of membrane-bound and intracellular signal transduction proteins in bacteria: Bacterial IQ, extroverts and introverts. BMC Microbiol. 2005;5: 1–19. doi:10.1186/1471-2180-5-35/FIGURES/5

51. Bell TH, Bell T. Many roads to bacterial generalism. FEMS Microbiol Ecol. 2021;97: 240. doi:10.1093/FEMSEC/FIAA240

52. Bury-Moné S, Kaakoush NO, Asencio C, Mégraud F, Thibonnier M, De Reuse H, et al. Is Helicobacter pylori a True Microaerophile? Helicobacter. 2006;11: 296–303. doi:10.1111/J.1523-5378.2006.00413.X

53. Pelliciari S, Pinatel E, Vannini A, Peano C, Puccio S, De Bellis G, et al. Insight into the essential role of the Helicobacter pylori HP1043 orphan response regulator: genome-wide identification and characterization of the DNA-binding sites. Sci Reports 2017 71. 2017;7: 1–15. doi:10.1038/srep41063

54. Olekhnovich IN, Vitko S, Valliere M, Hoffmana PS. Response to metronidazole and oxidative stress is mediated through homeostatic regulator hsra (hp1043) in helicobacter pylori. J Bacteriol. 2014;196: 729–739. doi:10.1128/JB.01047-13/ASSET/3730B1F4-D55B-43C0-9D6E-5BAD3A5E28BE/ASSETS/GRAPHIC/ZJB9990930210010.JPEG

55. Loh JT, Shum M V., Jossart SDR, Campbell AM, Sawhney N, Hayes McDonald W, et al. Delineation of the pH-responsive regulon controlled by the Helicobacter pylori ArsRS two-component system. Infect Immun. 2021;89. doi:10.1128/IAI.00597-20/SUPPL_FILE/IAI.00597-20-S0003.XLSX

56. Vannini A, Pinatel E, Costantini PE, Pelliciari S, Roncarati D, Puccio S, et al. Comprehensive mapping of the Helicobacter pylori NikR regulon provides new insights in bacterial nickel responses. Sci Reports 2017 71. 2017;7: 1–14. doi:10.1038/srep45458

57. Gölz G, Kittler S, Malakauskas M, Alter T. Survival of Campylobacter in the Food Chain and the Environment. Curr Clin Microbiol Reports. 2018;5: 126–134. doi:10.1007/S40588-018-0092-Z/METRICS

58. Dufour V, Li J, Flint A, Rosenfeld E, Rivoal K, Georgeault S, et al. Inactivation of the LysR regulator Cj1000 of Campylobacter jejuni affects host colonization and respiration. Microbiol (United Kingdom). 2013;159: 1165–1178. doi:10.1099/MIC.0.062992-0/CITE/REFWORKS

59. Svensson SL, Hyunh S, Parker CT, Gaynor EC. The Campylobacter jejuniCprRS two-component regulatory system regulates aspects of the cell envelope. Mol Microbiol. 2015;96: 189–209. doi:10.1111/MMI.12927/SUPPINFO

60. Fields JA, Li J, Gulbronson CJ, Hendrixson DR, Thompson SA. Campylobacter jejuni CsrA Regulates Metabolic and Virulence Associated Proteins and Is Necessary for Mouse Colonization. PLoS One. 2016;11: e0156932. doi:10.1371/JOURNAL.PONE.0156932
61. Price EE, Román-Rodríguez F, Boyd JM. Bacterial approaches to sensing and responding to respiration and respiration metabolites. Mol Microbiol. 2021;116: 1009–1021. doi:10.1111/MMI.14795
62. Sinha R, LeVeque RM, Callahan SM, Chatterjee S, Stopnisek N, Kuipel M, et al. Gut metabolite L-lactate supports Campylobacter jejuni population expansion during acute infection. Proc Natl Acad Sci. 2024;121: e2316540120. doi:10.1073/PNAS.2316540120
63. Contreras M, Thiberge JM, Mandrand-Berthelot MA, Labigne A. Characterization of the roles of NikR, a nickel-responsive pleiotropic autoregulator of Helicobacter pylori. Mol Microbiol. 2003;49: 947–963. doi:10.1046/J.1365-2958.2003.03621.X
64. Atabay HI, Corry JEL. Evaluation of a new arcobacter enrichment medium and comparison with two media developed for enrichment of Campylobacter spp. Int J Food Microbiol. 1998;41: 53–58. doi:10.1016/S0168-1605(98)00034-8
65. Beauchamp JM, Leveque RM, Dawid S, DiRita VJ. Methylation-dependent DNA discrimination in natural transformation of Campylobacter jejuni. Proc Natl Acad Sci U S A. 2017;114: E8053–E8061. doi:10.1073/PNAS.1703331114/-/DCSUPPLEMENTAL
66. Gibson DG, Young L, Chuang RY, Venter JC, Hutchison CA, Smith HO. Enzymatic assembly of DNA molecules up to several hundred kilobases. Nat Methods 2009 65. 2009;6: 343–345. doi:10.1038/nmeth.1318
67. Dalia AB, McDonough E, Camilli A. Multiplex genome editing by natural transformation. Proc Natl Acad Sci U S A. 2014;111: 8937–8942. doi:10.1073/pnas.1406478111
68. Cieślak M. Construction of the plasmid for the analysis of the essentiality of the Abu0127 gene for the survival of Arcobacter butzleri RM4018. Wroclaw University of Science and Technology -. 2021.
69. Perkins A, Tudorica DA, Amieva MR, James Remington S, Guillemin K. Helicobacter pylori senses bleach (HOCl) as a chemoattractant using a cytosolic chemoreceptor. PLOS Biol. 2019;17: e3000395. doi:10.1371/JOURNAL.PBIO.3000395
70. Langmead B, Salzberg SL. Fast gapped-read alignment with Bowtie 2. Nat Methods 2012 94. 2012;9: 357–359. doi:10.1038/nmeth.1923
71. Langmead B, Wilks C, Antonescu V, Charles R. Scaling read aligners to hundreds of threads on general-purpose processors. Bioinformatics. 2019;35: 421–432. doi:10.1093/BIOINFORMATICS/BTY648
72. Li H, Handsaker B, Wysoker A, Fennell T, Ruan J, Homer N, et al. The Sequence Alignment/Map format and SAMtools. Bioinformatics. 2009;25: 2078–2079. doi:10.1093/BIOINFORMATICS/BTP352
73. Liao Y, Smyth GK, Shi W. The R package Rsubread is easier, faster, cheaper and better for alignment and quantification of RNA sequencing reads. Nucleic Acids Res. 2019;47. doi:10.1093/NAR/GKZ114
74. Robinson MD, McCarthy DJ, Smyth GK. edgeR: a Bioconductor package for differential expression analysis of digital gene expression data. Bioinformatics. 2010;26: 139–140. doi:10.1093/BIOINFORMATICS/BTP616
75. Chen Y, Lun ATL, Smyth GK. From reads to genes to pathways: Differential expression analysis of RNA-Seq experiments using Rsubread and the edgeR quasi-likelihood pipeline. F1000Research. 2016;5. doi:10.12688/F1000RESEARCH.8987.2/DOI
76. Kevin Blighe SR. EnhancedVolcano: publication-ready volcano plots with enhanced colouring and labeling. [cited 21 Aug 2022]. Available: https://bioconductor.org/packages/devel/bioc/vignettes/EnhancedVolcano/inst/doc/EnhancedVolcano.html
77. Abele M, Doll E, Bayer FP, Meng C, Lomp N, Neuhaus K, et al. Unified workflow for the rapid and in-depth characterization of bacterial proteomes. Mol Cell Proteomics. 2023;22: 100612. doi:10.1016/j.mcpro.2023.100612
78. Doellinger J, Schneider A, Hoeller M, Lasch P. Sample Preparation by Easy Extraction and Digestion (SPEED) - A Universal, Rapid, and Detergent-free Protocol for Proteomics Based on Acid Extraction. Mol Cell Proteomics. 2020;19: 209–222. doi:10.1074/MCP.TIR119.001616
79. Cox J, Neuhauser N, Michalski A, Scheltema RA, Olsen J V., Mann M. Andromeda: a peptide search engine integrated into the MaxQuant environment. J Proteome Res. 2011;10: 1794–1805. doi:10.1021/PR101065J
80. Tyanova S, Temu T, Cox J. The MaxQuant computational platform for mass spectrometry-based shotgun proteomics. Nat Protoc 2016 1112. 2016;11: 2301–2319. doi:10.1038/nprot.2016.136

81. Cox J, Hein MY, Luber CA, Paron I, Nagaraj N, Mann M. Accurate proteome-wide label-free quantification by delayed normalization and maximal peptide ratio extraction, termed MaxLFQ. Mol Cell Proteomics. 2014;13: 2513–2526. doi:10.1074/MCP.M113.031591
82. Benjamini Y, Hochberg Y. Controlling the False Discovery Rate: A Practical and Powerful Approach to Multiple Testing. J R Stat Soc Ser B. 1995;57: 289–300. doi:10.1111/J.2517-6161.1995.TB02031.X
83. GitHub - mengchen18/omicsViewer. [cited 23 Jan 2024]. Available: https://github.com/mengchen18/omicsViewer
84. Kanehisa M, Furumichi M, Tanabe M, Sato Y, Morishima K. KEGG: new perspectives on genomes, pathways, diseases and drugs. Nucleic Acids Res. 2017;45: D353–D361. doi:10.1093/NAR/GKW1092
85. Huerta-Cepas J, Szklarczyk D, Heller D, Hernández-Plaza A, Forslund SK, Cook H, et al. eggNOG 5.0: a hierarchical, functionally and phylogenetically annotated orthology resource based on 5090 organisms and 2502 viruses. Nucleic Acids Res. 2019;47: D309–D314. doi:10.1093/NAR/GKY1085
86. Galperin MY, Makarova KS, Wolf YI, Koonin E V. Expanded microbial genome coverage and improved protein family annotation in the COG database. Nucleic Acids Res. 2015;43: D261–D269. doi:10.1093/NAR/GKU1223
87. Perez-Riverol Y, Bai J, Bandla C, García-Seisdedos D, Hewapathirana S, Kamatchinathan S, et al. The PRIDE database resources in 2022: a hub for mass spectrometry-based proteomics evidences. Nucleic Acids Res. 2022;50: D543–D552. doi:10.1093/NAR/GKAB1038

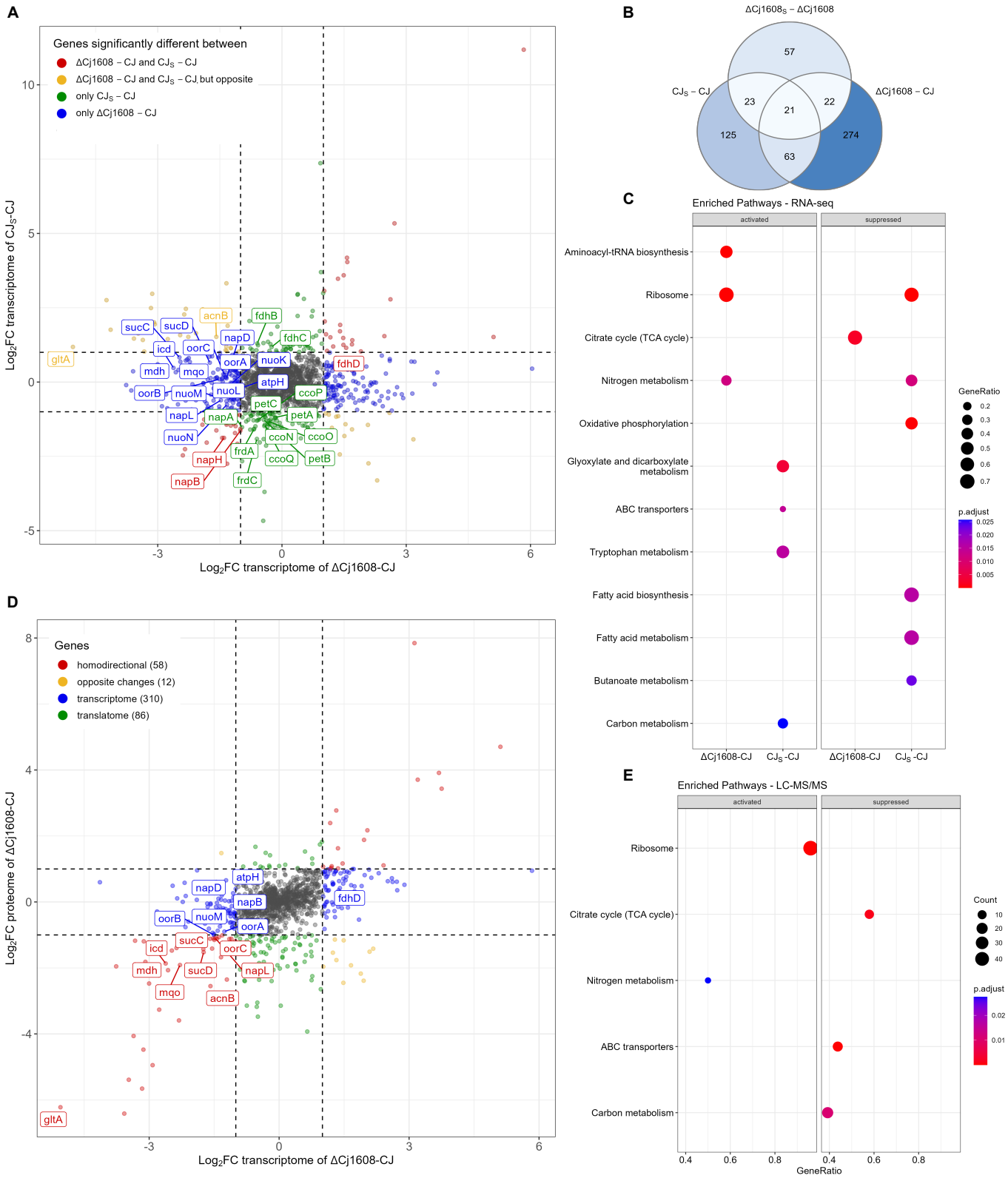
A
Genes significantly different between
ΔCj1608 – CJ and CJS – CJ
ΔCj1608 – CJ and CJS – CJ but opposite
only CJS – CJ
only ΔCj1608 – CJ
Log2FC transcriptome of CJS-CJ
Log2FC transcriptome of ΔCj1608-CJ
B
ΔCj1608S – ΔCj1608
CJS – CJ
ΔCj1608 – CJ
57
23
21
22
125
274
63
C
Enriched Pathways - RNA-seq
activated
suppressed
Aminoacyl-tRNA biosynthesis
Ribosome
Citrate cycle (TCA cycle)
Nitrogen metabolism
Oxidative phosphorylation
Glyoxylate and dicarboxylate metabolism
ABC transporters
Tryptophan metabolism
Fatty acid biosynthesis
Fatty acid metabolism
Butanoate metabolism
Carbon metabolism
ΔCj1608-CJ
CJS -CJ
GeneRatio
p.adjust
D
Genes
homodirectional (58)
opposite changes (12)
transcriptome (310)
translatome (86)
Log2FC proteome of ΔCj1608-CJ
Log2FC transcriptome of ΔCj1608-CJ
E
Enriched Pathways - LC-MS/MS
activated
suppressed
Ribosome
Citrate cycle (TCA cycle)
Nitrogen metabolism
ABC transporters
Carbon metabolism
GeneRatio
Count
p.adjust

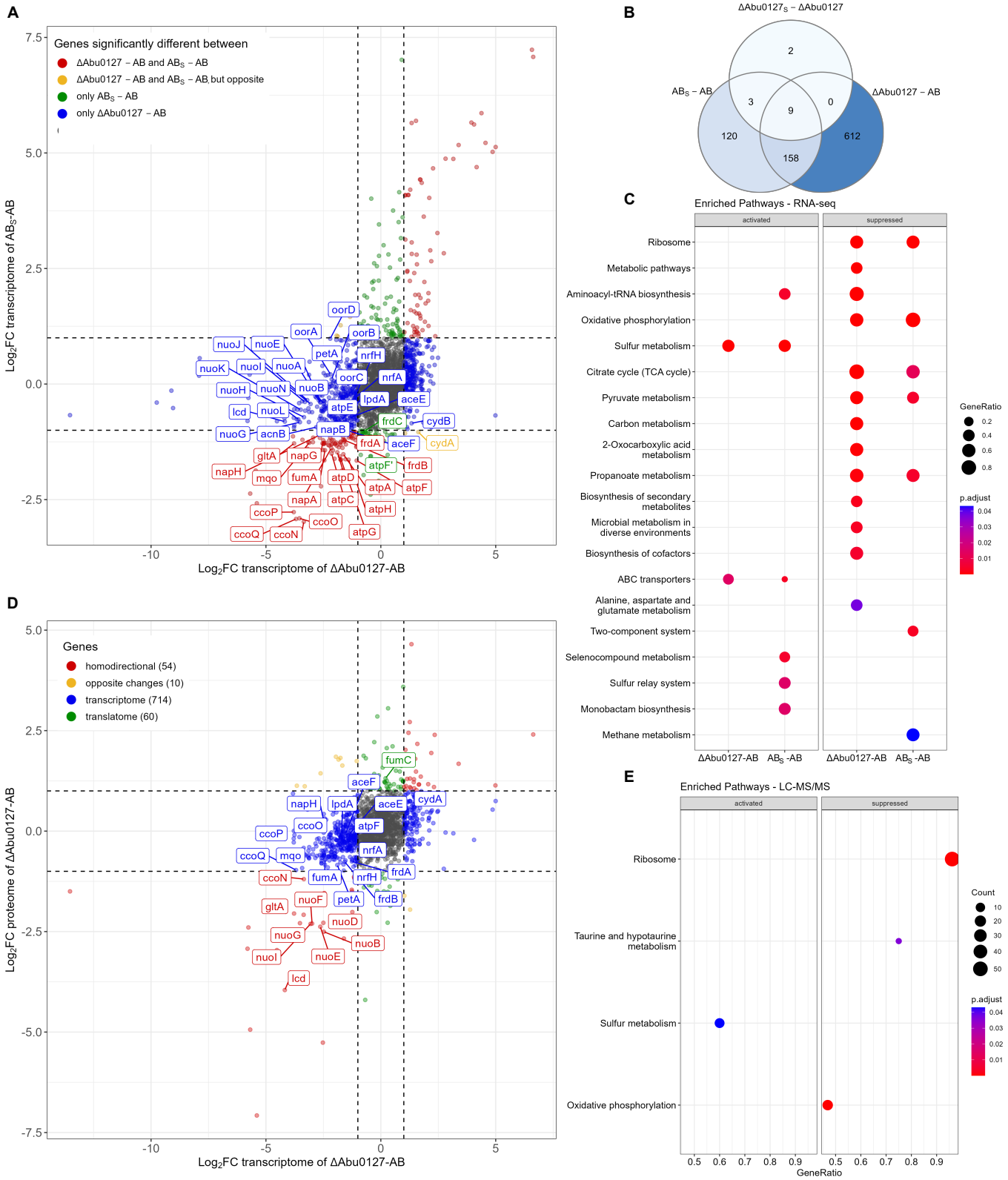
A
Genes significantly different between
ΔAbu0127 – AB and ABS – AB
ΔAbu0127 – AB and ABS – AB, but opposite
only ABS – AB
only ΔAbu0127 – AB
Log2FC transcriptome of ABS-AB
Log2FC transcriptome of ΔAbu0127-AB
B
ΔAbu0127S – ΔAbu0127
ABS – AB
ΔAbu0127 – AB
2
3
9
0
120
612
158
C
Enriched Pathways - RNA-seq
activated
suppressed
Ribosome
Metabolic pathways
Aminoacyl-tRNA biosynthesis
Oxidative phosphorylation
Sulfur metabolism
Citrate cycle (TCA cycle)
Pyruvate metabolism
Carbon metabolism
2-Oxocarboxylic acid metabolism
Propanoate metabolism
Biosynthesis of secondary metabolites
Microbial metabolism in diverse environments
Biosynthesis of cofactors
ABC transporters
Alanine, aspartate and glutamate metabolism
Two-component system
Selenocompound metabolism
Sulfur relay system
Monobactam biosynthesis
Methane metabolism
ΔAbu0127-AB
ABS -AB
GeneRatio
p.adjust
D
Genes
homodirectional (54)
opposite changes (10)
transcriptome (714)
translatome (60)
Log2FC proteome of ΔAbu0127-AB
Log2FC transcriptome of ΔAbu0127-AB
E
Enriched Pathways - LC-MS/MS
activated
suppressed
Ribosome
Taurine and hypotaurine metabolism
Sulfur metabolism
Oxidative phosphorylation
GeneRatio
Count
p.adjust

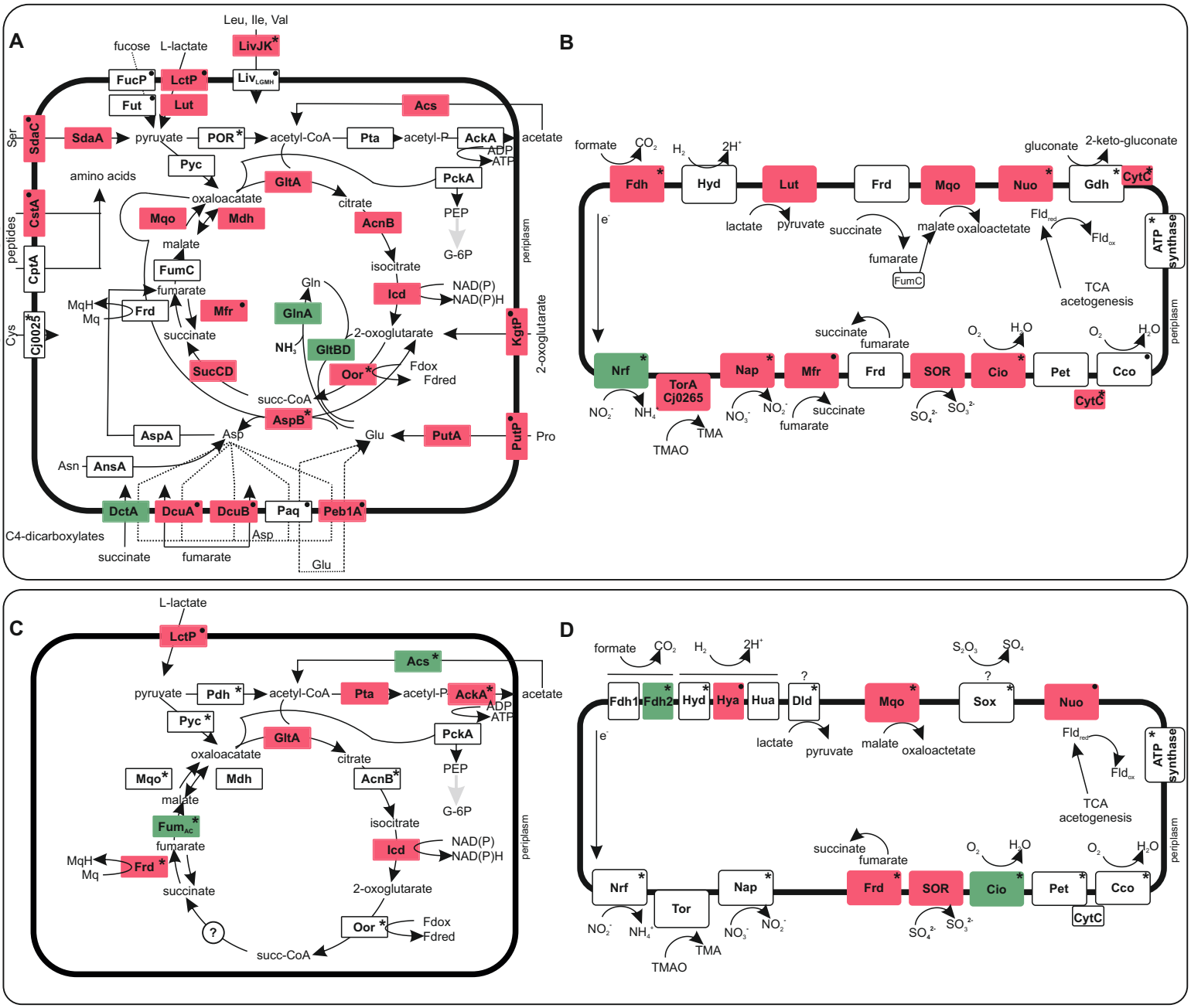
Campylobacter jejuni
A
Leu, Ile, Val
LivJK*
fucose
L-lactate
FucP
LctP
Liv LGMH
Fut
Lut
Acs
Ser
SdaC
SdaA
pyruvate
POR*
acetyl-CoA
Pta
acetyl-P
AckA
acetate
ADP
ATP
Pyc
amino acids
GltA
PckA
oxaloacetate
citrate
PEP
CstA
Mqo
Mdh
AcnB
G-6P
peptides
malate
FumC
isocitrate
CptA
fumarate
Gln
Icd
NAD(P)
NAD(P)H
MqH
Mq
Frd
Mfr
GlnA
2-oxoglutarate
KgtP
Cys
Cj0025
succinate
NH3
GltBD
SucCD
Oor*
Fdox
Fdred
succ-CoA
AspB*
AspA
Asp
Glu
PutA
PutP
Pro
periplasm
2-oxoglutarate
Asn
AnsA
DctA
DcuA
DcuB
Paq
Peb1A
C4-dicarboxylates
succinate
fumarate
Asp
Glu
B
formate
CO2
H2
2H+
Fdh*
Hyd
Lut
Frd
Mqo
Nuo*
gluconate
2-keto-gluconate
Gdh*
CytC*
e-
lactate
pyruvate
succinate
malate
oxaloactetate
Fld red
Fld ox
ATP synthase
fumarate
FumC
TCA
acetogenesis
succinate
fumarate
O2
H2O
Nrf*
TorA
Cj0265
Nap*
Mfr
Frd
SOR
Cio*
Pet
Cco
CytC*
NO2-
NH4+
NO3-
NO2-
succinate
fumarate
SO4 2-
SO3 2-
TMA
TMAO
periplasm
Arcobacter butzleri
C
L-lactate
LctP
Acs*
pyruvate
Pdh*
acetyl-CoA
Pta
acetyl-P
AckA*
acetate
ADP
ATP
Pyc*
GltA
PckA
oxaloacetate
citrate
PEP
Mqo*
Mdh
AcnB*
G-6P
malate
Fum AC*
isocitrate
fumarate
Icd
NAD(P)
NAD(P)H
MqH
Mq
Frd*
succinate
2-oxoglutarate
?
Oor*
Fdox
Fdred
succ-CoA
periplasm
D
formate
CO2
H2
2H+
S2O3
SO4
Fdh1
Fdh2*
Hyd*
Hya
Hua
Dld*
?
Mqo*
Sox*
Nuo
e-
lactate
pyruvate
malate
oxaloactetate
Fld red
Fld ox
ATP synthase
TCA
acetogenesis
succinate
fumarate
O2
H2O
Nrf*
Tor
Nap*
Frd*
SOR
Cio*
Pet*
Cco*
CytC
NO2-
NH4+
NO3-
NO2-
SO4 2-
SO3 2-
TMA
TMAO
periplasm
repressed in ΔCj1608/ΔAbu0127
activated in ΔCj1608/ΔAbu0127
unchanged in ΔCj1608/ΔAbu0127
gluconeogenesis, none of the proteins changed significantly
undetected or partially detected by MS
* see Supplementary Data 1-3 for comprehensive results
? unknown or putative

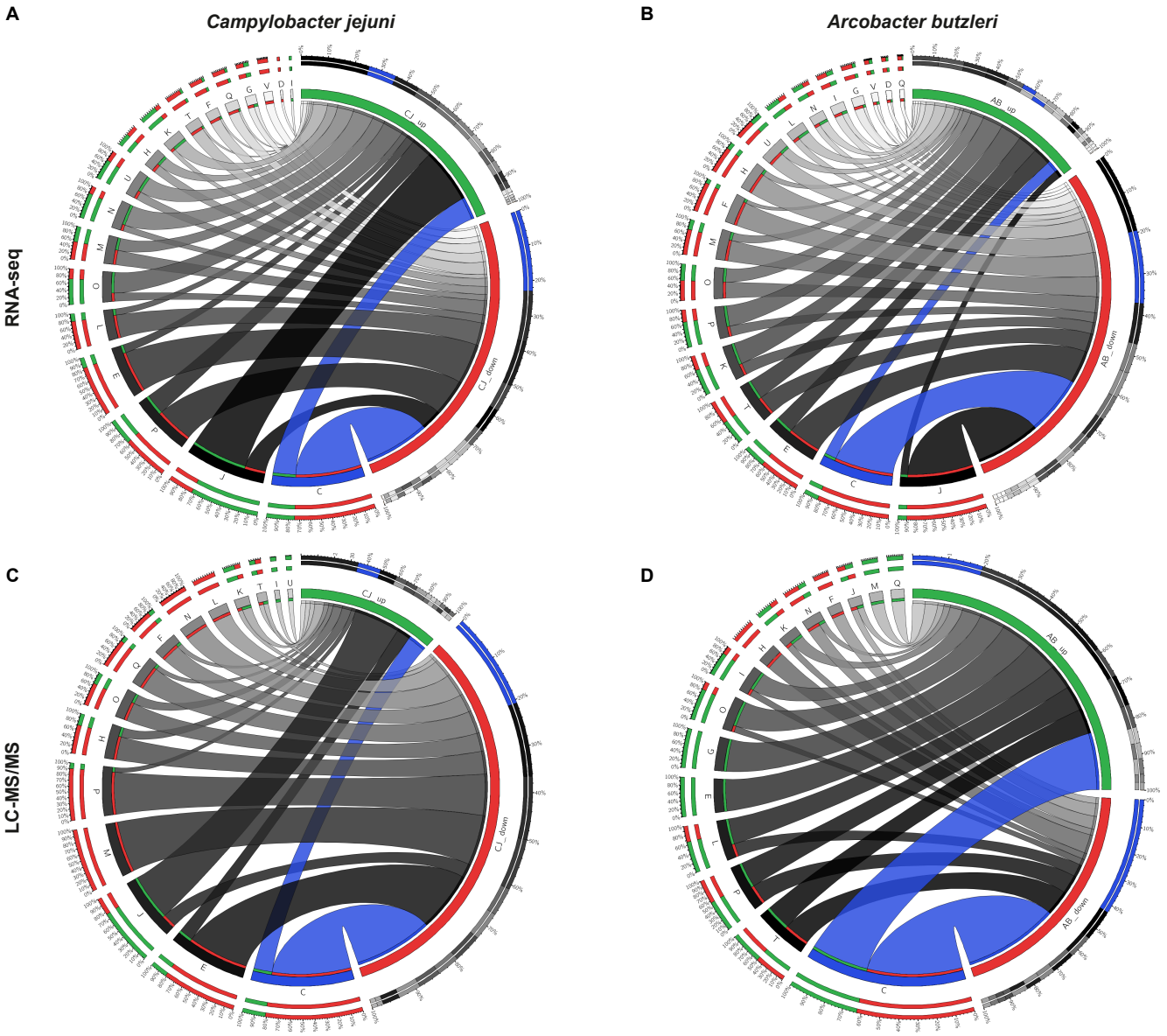

C - energy production and conversion, **D** - cell cycle control, cell division, chromosome partitioning, **E** - amino acid transport and metabolism, **F** - nucleotide transport and metabolism, **G** - carbohydrate transport and metabolism, **H** - coenzyme transport and metabolism, **I** - lipid transport and metabolism, **J** - translation, ribosomal structure and biogenesis, **K** - transcription, **L** - replication, recombination and repair, **M** - cell wall/membrane/envelope biogenesis, **N** - cell motility, **O** - posttranslational modification, protein turnover, chaperones , **P** - inorganic ion transport and metabolism, **Q** - secondary metabolites biosynthesis, transport and catabolism, **T** - signal transduction mechanisms, **U** - intracellular trafficking, secretion, and vesicular transport, **V** - defense mechanisms

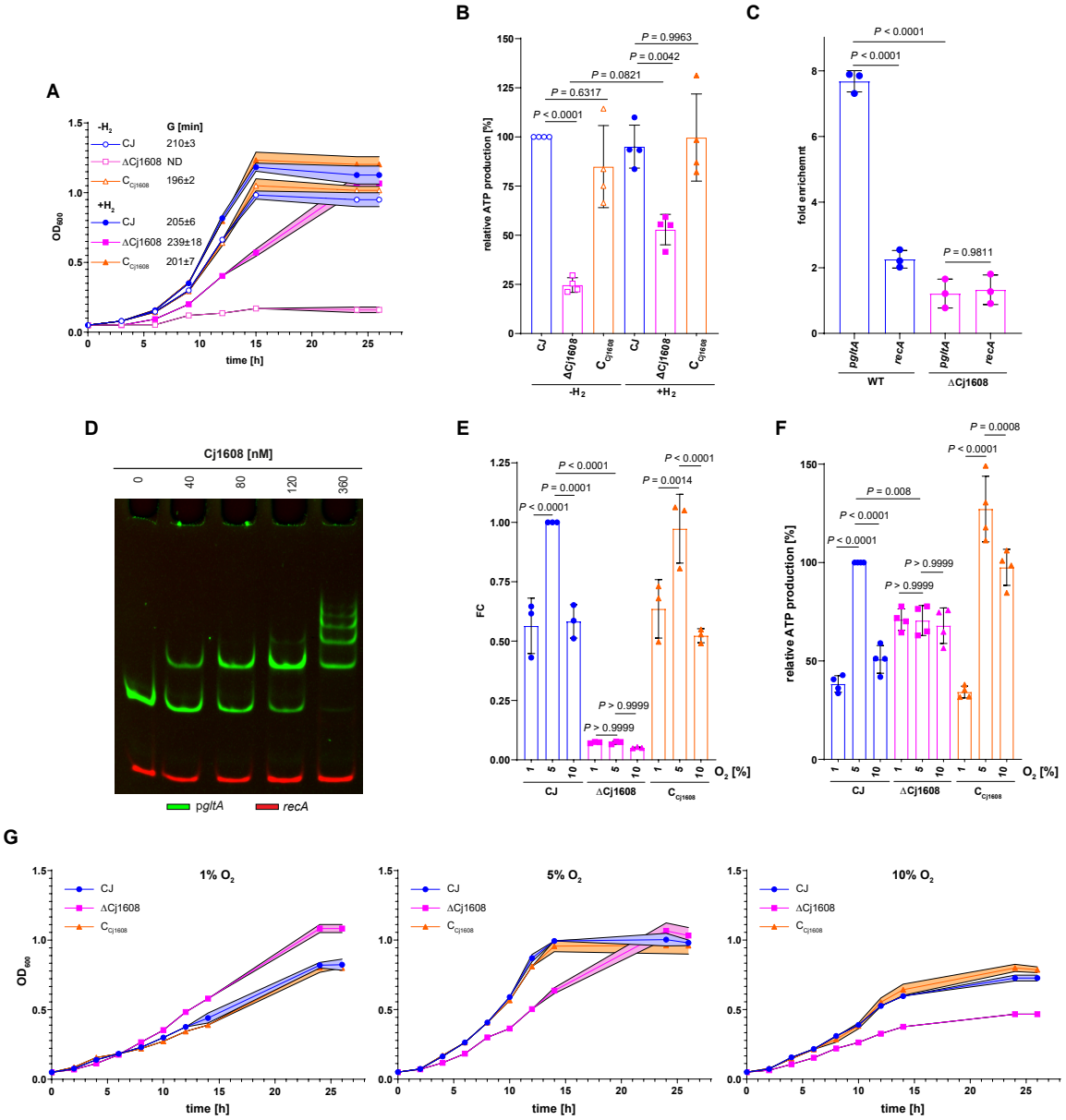
A
-H2
G [min]
CJ 210±3
ΔCj1608 ND
CCj1608 196±2
+H2
CJ 205±6
ΔCj1608 239±18
CCj1608 201±7
OD600
time [h]
B
relative ATP production [%]
P < 0.0001
P = 0.6317
P = 0.0821
P = 0.0042
P = 0.9963
CJ
ΔCj1608
CCj1608
-H2
+H2
C
fold enrichemnt
P < 0.0001
P < 0.0001
P = 0.9811
pgltA
recA
WT
ΔCj1608
D
Cj1608 [nM]
0
40
80
120
360
pgltA
recA
E
FC
P < 0.0001
P = 0.0001
P < 0.0001
P > 0.9999
P > 0.9999
P < 0.0001
P = 0.0014
O2 [%]
CJ
ΔCj1608
CCj1608
F
relative ATP production [%]
P = 0.0008
P < 0.0001
P = 0.008
P < 0.0001
P < 0.0001
P > 0.9999
P > 0.9999
O2 [%]
CJ
ΔCj1608
CCj1608
G
1% O2
5% O2
10% O2
CJ
ΔCj1608
CCj1608
OD600
time [h]

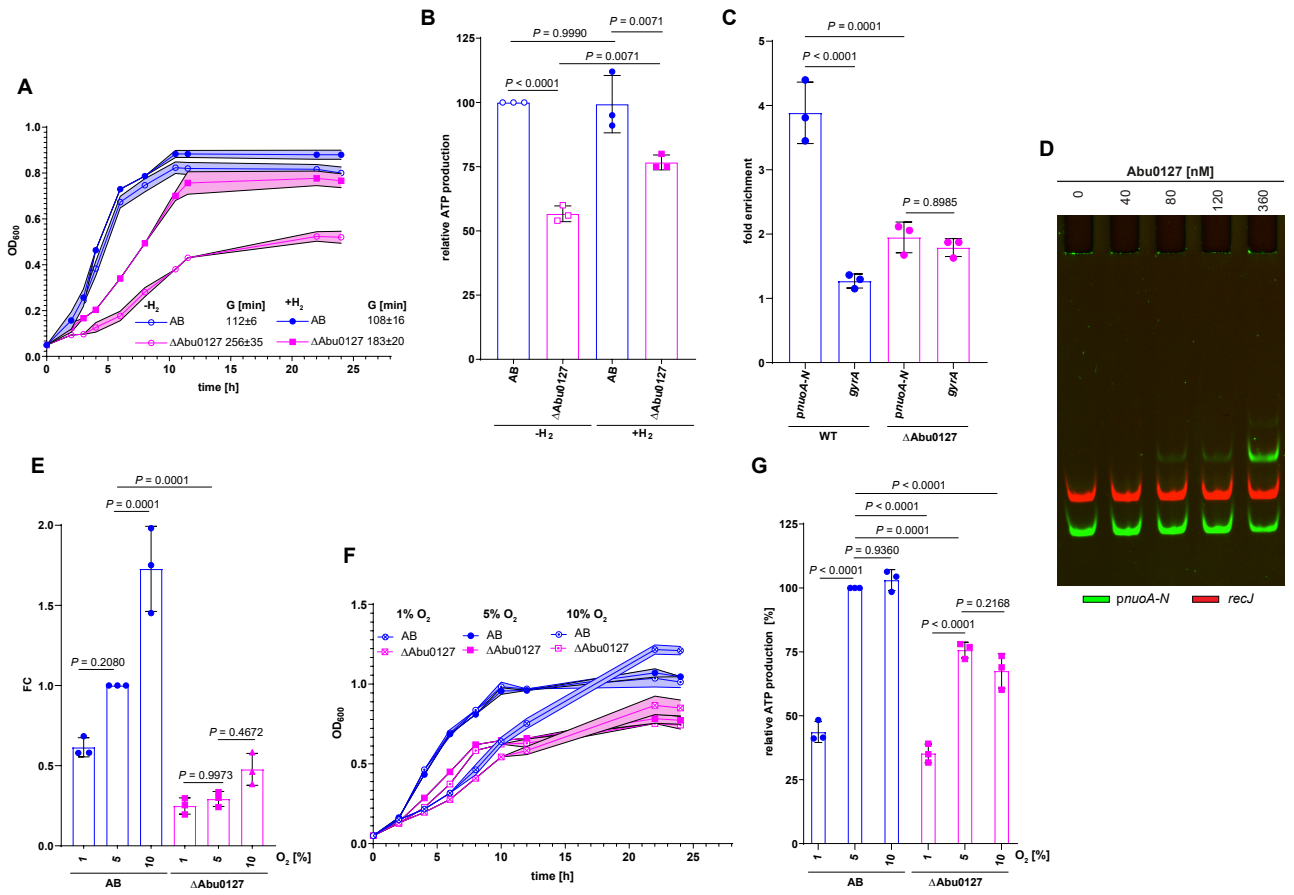
A
OD600
time [h]
-H2
AB
ΔAbu0127
G [min]
112±6
256±35
+H2
AB
ΔAbu0127
G [min]
108±16
183±20
B
relative ATP production
P = 0.9990
P = 0.0071
P = 0.0071
P < 0.0001
AB
ΔAbu0127
AB
ΔAbu0127
-H2
+H2
C
fold enrichment
P = 0.0001
P < 0.0001
P = 0.8985
pnuoA-N
gyrA
pnuoA-N
gyrA
WT
ΔAbu0127
D
Abu0127 [nM]
0
40
80
120
360
pnuoA-N
recJ
E
FC
P = 0.0001
P = 0.0001
P = 0.2080
P = 0.4672
P = 0.9973
O2 [%]
AB
ΔAbu0127
F
1% O2
5% O2
10% O2
AB
ΔAbu0127
OD600
time [h]
G
relative ATP production [%]
P < 0.0001
P < 0.0001
P = 0.0001
P = 0.9360
P < 0.0001
P = 0.2168
P < 0.0001
O2 [%]
AB
ΔAbu0127